NASA/TM—2005-214030

Moisture-Induced Spallation and Interfacial Hydrogen Embrittlement of Alumina Scales

James L. Smialek
Glenn Research Center, Cleveland, Ohio

December 2005

The NASA STI Program Office . . . in Profile

Since its founding, NASA has been dedicated to the advancement of aeronautics and space science. The NASA Scientific and Technical Information (STI) Program Office plays a key part in helping NASA maintain this important role.

The NASA STI Program Office is operated by Langley Research Center, the Lead Center for NASA's scientific and technical information. The NASA STI Program Office provides access to the NASA STI Database, the largest collection of aeronautical and space science STI in the world. The Program Office is also NASA's institutional mechanism for disseminating the results of its research and development activities. These results are published by NASA in the NASA STI Report Series, which includes the following report types:

- TECHNICAL PUBLICATION. Reports of completed research or a major significant phase of research that present the results of NASA programs and include extensive data or theoretical analysis. Includes compilations of significant scientific and technical data and information deemed to be of continuing reference value. NASA's counterpart of peer-reviewed formal professional papers but has less stringent limitations on manuscript length and extent of graphic presentations.

- TECHNICAL MEMORANDUM. Scientific and technical findings that are preliminary or of specialized interest, e.g., quick release reports, working papers, and bibliographies that contain minimal annotation. Does not contain extensive analysis.

- CONTRACTOR REPORT. Scientific and technical findings by NASA-sponsored contractors and grantees.

- CONFERENCE PUBLICATION. Collected papers from scientific and technical conferences, symposia, seminars, or other meetings sponsored or cosponsored by NASA.

- SPECIAL PUBLICATION. Scientific, technical, or historical information from NASA programs, projects, and missions, often concerned with subjects having substantial public interest.

- TECHNICAL TRANSLATION. English-language translations of foreign scientific and technical material pertinent to NASA's mission.

Specialized services that complement the STI Program Office's diverse offerings include creating custom thesauri, building customized databases, organizing and publishing research results . . . even providing videos.

For more information about the NASA STI Program Office, see the following:

- Access the NASA STI Program Home Page at ***http://www.sti.nasa.gov***

- E-mail your question via the Internet to help@sti.nasa.gov

- Fax your question to the NASA Access Help Desk at 301–621–0134

- Telephone the NASA Access Help Desk at 301–621–0390

- Write to:
  NASA Access Help Desk
  NASA Center for AeroSpace Information
  7121 Standard Drive
  Hanover, MD 21076

NASA/TM—2005-214030

Moisture-Induced Spallation and Interfacial Hydrogen Embrittlement of Alumina Scales

James L. Smialek
Glenn Research Center, Cleveland, Ohio

Prepared for
High Temperature Corrosion
sponsored by Gordon Research Conferences
New London, New Hampshire, July 24–29, 2005

National Aeronautics and
Space Administration

Glenn Research Center

December 2005

Available from

NASA Center for Aerospace Information
7121 Standard Drive
Hanover, MD 21076

National Technical Information Service
5285 Port Royal Road
Springfield, VA 22100

Available electronically at http://gltrs.grc.nasa.gov

Moisture-Induced Spallation and Interfacial Hydrogen Embrittlement of Alumina Scales

James L. Smialek
National Aeronautics and Space Administration
Glenn Research Center
Cleveland, Ohio 44135

Abstract

Thermal expansion mismatch stresses and interfacial sulfur activity are the major factors producing primary Al_2O_3 scale spallation on high temperature alloys. However, moisture-induced delayed spallation appears as a secondary, but often dramatic, illustration of an additional mechanistic detail. A historical review of delayed failure of alumina scales and TBC's on superalloys is presented herein. Similarities with metallic phenomena suggest that hydrogen embrittlement from ambient humidity, resulting from the reaction $Al+3H_2O=Al(OH)_3+3H^+ +3e^-$, is the operative mechanism. This proposal was tested by standard cathodic hydrogen charging in 1N H_2SO_4, applied to René N5 pre-oxidized at 1150 °C for 1000 1-hr cycles, and monitored by weight change, induced current, and microstructure. Here cathodic polarization at –2.0 V abruptly stripped mature Al_2O_3 scales at the oxide-metal interface. Anodic polarization at 2.0 V, however, produced alloy dissolution. Finally, with no applied voltage, the electrolyte alone produced neither scale spallation nor alloy dissolution. These experiments thus highlight the detrimental effects of hydrogen charging on alumina scale adhesion. It is proposed that interfacial hydrogen embrittlement is produced by moist air and is the root cause of both moisture-induced, delayed scale spallation and desktop TBC failures.

Introduction

High temperature turbine materials rely on the formation of protective scales for durable operation. Specifically, single crystal Ni-based superalloy airfoils are usually coated with aluminide conversion coatings of Ni(Pt)Al or with overlay Ni(Co)CrAlY coatings, both producing slow growing, adherent α-Al_2O_3 scales. These coatings may also be used as bond coatings beneath YSZ (yttria stabilized zirconia) thermal barrier coatings (TBC), whose cyclic life depends on maintaining these same beneficial properties of the intermediate thermally grown oxide (TGO). Cyclic oxidation tests are often used to characterize the oxidative stability of both the bond coat class of materials alone, as well as the TBC system as a whole. Scale adhesion is maximized by using low sulfur (<1 ppmw) coatings and alloys, as well as Pt additions and reactive element dopants (e.g., ~0.1% Y, Hf, Zr). It is well recognized that the primary driving force for scale and TBC spallation is their low thermal expansion, compared to the metal substrate, and the high biaxial compressive thermal mismatch stress and strain energy that results on cool-down. However a secondary factor affecting failure of the scale or TBC may be moisture in the ambient air, especially in the case of damaged or marginally adherent scales. Secondary, or delayed, moisture-induced scale failure is the subject of this study.

Related Experience at NASA GRC

A. Bulk Alloys and Uncoated Single Crystal Superalloys

NiCrAl

Alumina scale spallation due to thermal cycling is widely recognized to depend on interfacial sulfur segregation. But when the scale is near failure, due to marginally high sulfur contents coupled with large

stored strain energy, it also becomes noticeably susceptible to moisture (refs. 1 to 7). Our earliest demonstration of this phenomenon was nearly 20 years ago during the first demonstration of increased scale adhesion with sulfur removal (ref. 1). In these "purging" experiments, a model undoped Ni-15Cr-13Al (wt%) alloy was repeatedly oxidized for 1 hr at 1120 °C, weighed, then lightly polished on wet 600 grit emery to just remove the scale. Since sulfur interfacial segregation was believed to cause scale spallation, removing the scale was expected to also remove the segregated sulfur.

The first few oxidation/polishing cycles showed classic, massive Al_2O_3 scale spallation, with weight loss on each cycle. But after 8 such cycles, the weight loss was reduced, and transitioned to a weight gain at 10 cycles and complete, repetitive scale adhesion at 13 cycles (fig. 1). Subsequently, however, upon initial exposure to water during the wet sanding process, the scale was observed to completely peel off. A macrograph for samples purged for 15 cycles, illustrating the striking contrast in retained scale between the as-cooled and the water exposed sample, is shown in figure 2. The effect of moisture was to almost completely strip an otherwise intact scale.

This moisture effect was further monitored by plotting the weight change for each cycle before and after water exposure (fig. 3). Here some scatter exists in measuring the small weight change for just one hour heating, after repolishing each cycle. But it is clear that small weight losses or no changes occur when the scale spalled for the first ten cycles, while trending into more adhesion and eventual weight gains with more purging cycles. After 10 cycles, the net weight change after immersion indicates spallation of an originally intact scale. The extent of water-induced spallation is thus portrayed as the shaded area between the two curves. Finally, at 24 to 25 cycles, enough sulfur has been removed, decreasing from 10 down to 2 ppmw, allowing the scale to remain adherent even when exposed to water.

This experience sensitized us to the phenomenon of secondary (delayed) or moisture-induced spallation of marginally adherent Al_2O_3 scales. It encouraged us, in many subsequent studies of sulfur effects on scale adhesion, to adopt procedures of breathing on samples or spot testing by water immersion. This has often resulted in equally remarkable displays of water-induced spallation for single crystal superalloys, such as PWA 1480, PWA 1484, René 142, and René N5, known to be protected by an inner layer of α-Al_2O_3. The nominal compositions are listed in table I.

PWA 1480

The first demonstration of fully adherent scales on low sulfur single crystal superalloys was accomplished by desulfurizing PWA 1480 in 1 atm hydrogen (ref. 2). In this study, different degrees of sulfur removal were accomplished by hydrogen annealing for 100 hr at 1000 to 1300 °C. A subsequent study examined a more complete matrix of annealing times, temperatures and thicknesses (ref. 5). Since sulfur removal was completed only at the higher values of the sulfur diffusion product ($D_S t/L^2$), the less effective treatments still allowed moisture-induced spallation.

PWA 1484

Similar behavior was observed for PWA 1484 (refs. 5 and 8). Here the sulfur content was obtained at three levels, where the nominal casting contained 1.2 ppmw and was reduced down to 0.01 ppmw by hydrogen annealing in 5%H_2/Ar at 1250 °C for 50 hr. A low sulfur alloy was also produced commercially at 0.25 ppmw S by melt desulfurization. Cyclic oxidation at 1100 °C demonstrated excellent performance, showing little weight loss or interfacial spalling at the 0.25 and 0.01 ppmw sulfur levels (fig. 4). However, at 1.2 ppmw there was considerable spalling, with abrupt additional drops in weight at 400, 800, and 2000 hr indicating scale loss due to water immersion. Again this can be illustrated by before and after macrographs (fig. 5(a)). In contrast, the low sulfur, H_2-annealed sample was basically immune to moisture-induced spallation for the duration of the test (fig. 5(b)).

René 142

Long term cyclic oxidation at 1150 °C was performed on alloy René 142 (refs. 3 and 4). A substantial benefit was noted for samples annealed in 1 atm. H_2 at 1280 °C for 100 hr by reducing the sulfur content

from 6.1 down to 0.3 ppmw. However, despite relatively moderate weight losses after cycling the desulfurized sample for 1000 hr (fig. 6), further spallation was produced by moisture effects, i.e., breathing hot moist air on the samples after an initial weighing. The cumulative effect of such additional treatment can be seen as the upper curve. Its close symmetry to the net sample weight change is an indication of how moisture-induced secondary spallation may account for primary trends in the overall $\Delta W/A$ cyclic oxidation response. This spallation was also visibly apparent in the series of macrographs corresponding to moist air treatments after various oxidation times, for both as received René 142 and for samples desulfurized by annealing in 1 atm H_2 for 100 hr at 1280 °C (fig. 7(a) and (b)). Finally, the additional weight loss at 1000 hr, shown by the arrows in figure 6, was produced by water immersion after cooldown. This response is further illustrated in the before and after macrographs of figure 8.

René N5±Y

In those same studies, some René N5+Y samples would also, on occasion, exhibit moisture induced spallation (fig. 9) (refs. 3 and 4). In a subsequent study, water immersion of as-received (A.R.) René N5±15–100 ppmw Y samples produced interfacial scale spallation up to 1.5 mg/cm^2, for otherwise quite protective scales grown after 500 1-hr cycles at 1150 °C (ref. 6). This is shown by the additional weight loss in figure 10 and in the macrographs of figure 11(a). For a duplicate set of samples, hydrogen annealing in 5% H_2/Ar at 1250 °C for 100 hr has been shown to essentially eliminate this moisture effect, (fig. 11(b)), even though no desulfurization had occurred for the Y-doped set of alloys. Continuous monitoring by acoustic emission (AE), for a sample that had been at ambient conditions for a year, has shown that moisture-induced spallation can occur over long durations up to many hours, but with multiple events proceeding in discreet, consecutive, near instantaneous bursts (fig. 12) and (ref. 7). The moisture–induced AE response was more pronounced for the as-received samples compared to the duplicate H_2-annealed set, and reflects a 6 percent total spalled area compared to just 0.3 percent, respectively. Some discussion of the effect of decarburization of N5+Y during hydrogen annealing was offered as an explanation or at least as a correlation with improved scale adhesion.

B. Anecdotal TBC Experience

Along similar lines, it is often noted in cyclic furnace testing that the final catastrophic failure of a TBC does not occur immediately on cooldown, as expected when just reaching the maximum thermal expansion mismatch stresses. Rather, an incubation period of minutes, hours, or days is experienced before failure. We have often observed this failure, although delayed after cooldown, to be a near instantaneous event when it does occur.

Recently six commercially applied *EB-PVD* modified YSZ coatings, with a conventional Pt-aluminide bond coat on René N5, were furnace cycled between heating to 1135 °C for 45 min and cooling to 150 °C for 15 min. When failure occurred, it was usually manifested as quite destructive buckling or delamination events, well after cooldown was completed. Lifetimes ranged from 360 to 720 cycles **(**fig. 13). The failure locus of one sample was examined by XRD and SEM/EDS of the exposed sample surface. This revealed that only dispersed filaments of YSZ were retained on the sample and were attached to embedded islands of Al_2O_3. These features were scattered over the surface and entrained in depressions of a heavily convoluted, but otherwise cleanly exposed bond coat **(**fig. 14**)**. Thus the failure locus appears to occur primarily at the scale-metal interface, partly through embedded scale intrusions, but least through the YSZ itself. This reinforces the importance of scale-metal adhesion to TBC durability.

Plasma sprayed coatings have exhibited delamination in one intact free-standing wafer, seen in the macrographs of figure 15, rather than as the complex buckling and cracking shown above. Here a 250 μm thick coating of APS 8YSZ was applied to both sides of grit blasted coupons of PWA 1484 with no bond coat, then cycled between 1100 and 80 °C each hr (ref. 7). The lifetime of these coatings was closely related to the sulfur content of the alloy **(**fig. 16**)**, and it was therefore correlated with the cyclic oxidation

behavior of the companion uncoated coupons shown in figure 4. Nearly all coated faces failed by delayed "desktop spallation" (DTS), well after the samples had cooled to room temperature. On the lowest sulfur sample, 0.01 ppmw, one coated face survived 2000 1-hr cycles, only to fail in a subsequent room temperature water immersion test. While the failure locus was much more complex for the APS coatings, some areas of spalling to bare metal were observed, as shown in the SEM micrographs of figure 17. The associated role of sulfur on interfacial scale spallation here may thus be to initiate interfacial cracks and contribute to more general TBC failure.

Additional Moisture Effect Studies

A number of other published studies provide important documentation of the moisture effect on scale adhesion. Sigler showed that moisture, or synthetic exhaust gas containing 14 percent water, qualitatively increased alumina scale spallation on Fe-20Cr-5Al-X alloys (wt%) in 24 hr oxidation tests at 900 to 1150 °C (ref. 9). This was demonstrated for alloys doped with Ca, Mg, Y, Ce, and Ti. Sulfur content was not systematically varied, and no information was provided regarding the moisture effect on undoped FeCrAl.

Smith, Frazier, and Pregger oxidized René N6 in flowing gas (20% O_2 to 80% N_2), either dry or bubbled through water, at 1150 °C for 24 hr (ref. 10). A low 0.036 ppmw S alloy formed an adherent scale in either dry or moist air. The high 4.3 ppmw S alloy initially retained an adherent scale in the dry gas mixture, but the scale spalled when the sample was removed from the furnace and exposed to ambient air humidity. Additionally, this alloy spalled straightaway when oxidized and cooled in the moist furnace gas mixture. Other high sulfur samples managed to retain their scale. When bent in the vacuum of an Auger microscope, the scale remained adherent. When bent in air, they readily spalled. Low sulfur samples did not spall appreciably, even when bent in ambient air. Thus the sensitivity of alumina scales to moisture induced spallation is again demonstrated for marginally adherent cases.

Janakiraman, Meier, and Pettit conducted an extensive study of the effects of moisture on the 1100 °C cyclic oxidation of single crystal superalloys, using 45 min cycles, in furnaces whose atmospheres were fixed at $p_{H2O} = 6\times10^{-5}$ (dry) or 0.1 (wet) atm (ref. 11). Superalloys with sulfur contents greater than 3 ppmw showed substantially greater weight loss, 2 to 4 times that measured in dry air. In contrast, samples that were desulfurized in the melt or by subsequent hydrogen annealing to less than 1 ppmw were virtually immune to the moisture effect for times exceeding 3000 hr. Water droplet tests also showed increased spallation, which diminished as continued sulfur 'purging' was accomplished by a number of repeated oxidation/polishing treatments, as shown for NiCrAl in figure 3. It was unequivocally demonstrated that moisture effects on alumina spallation were only possible when the interface toughness was compromised by sulfur impurities. A mechanism of stress corrosion cracking and moisture effects on interfacial bonding and toughness was discussed.

Sergo and Clarke (ref. 12) have used photoluminescence piezospectroscopy to characterize the stress state of the interface scale at the edge of a buckled debonding region for an EB-PVD TBC on a NiCoCrAlY bond coated PWA 1484 sample. Tolpygo and Clarke used similar techniques to monitor Al_2O_3 buckle growth on oxidized FeCrAlZr (ref. 13). Both studies found that cracks and buckle progression could proceed over the course of days and attributed such subcritical crack growth to ambient moisture effects. Both studies serve to connect the delayed failure of alumina scales with TBC buckling.

Renusch, Eschler, and Schutze have recently documented long term AE activity after cooldown in ambient air for an oxidized APS TBC/NiCrAlY bond coated IN738 samples and attributed these events to cracking in the alumina scale (ref. 14). The hypothesis presented, regarding hydrogen embrittlement, is supported by their recent detection of hydrogen under Al_2O_3 scales using proton induced gamma emission PIGE (ref. 15). Here pre-oxidized samples were fractured in-situ high vacuum to expose the oxide-metal interface.

Hydrogen Embrittlement Experiment

Motivation

It was further recognized from the literature that moisture alone has also caused a similar puzzling detrimental effect in intermetallic compounds such as Ni_3Al and FeAl, ultimately identified as hydrogen embrittlement (refs. 16 to 20). Hydrogen embrittlement of single crystal superalloys has also been identified (refs. 21 and 22). Classic hydrogen embrittlement exhibits many features in common with delayed scale spallation: an interfacial aspect, an intermittent nature depending on hydrogen diffusion ahead of the crack tip, a necessity of a triaxial tension stress state, a negative synergy with segregated sulfur, and a reduction in the theoretical bond strength (refs. 23 and 25). We therefore postulate that the same underlying phenomenon controls delayed spallation in ambient air or by water immersion. Some remarkable analogies of scale spallation with alloy embrittlement by sulfur and hydrogen are listed in table II. This hypothesis was first presented, along with much of the forgoing circumstantial evidence and preliminary results, at a TMS symposium on water vapor effects on the high temperature oxidation of materials, and then elaborated at the TMS symposium on superalloy and coatings for high temperature applications (refs. 26 and 27). The paraphrased dictum shown here summarizes two precepts of a scientific rule, classically known as Occam's Razor, stating that: (1) the simplest competing theory be preferred to the more complex, and (2) new explanations of the unknown should be sought first in terms of known phenomena.

To test such a mechanism, a standard procedure was used to charge pre-oxidized René N5 samples with hydrogen, under the expectation that an excess of hydrogen would accentuate interfacial spalling for a damaged, highly stressed mature scale. From the literature, hydrogen charging is often accomplished electrolytically in S, P, or As poisoned H_2SO_4, at currents ≤150 mA/cm^2 and potentials ≤–2 V (Ag/AgCl) (refs. 16 and 25). Our simple charging cell is shown schematically in figure 18, using only a 0.020 in. Pt wire counter-electrode without a reference electrode. The working electrode consisted of 1.3×2.5 cm N5 samples suspended from a Pt wire, submerged about halfway into the 500 ml solution. The bottom edge was sanded to insure a conductive path. A constant voltage power supply was used to apply a potential, while cell current was measured using a precision potentiometer across a low resistance load of 1 ohm.

Duplicate N5 samples were exposed to a constant positive or negative potential and monitored for response by current, weight change, surface macro and microstructure. The potentials were chosen based on the general response of a bare control sample. Scanning electron microscopy (SEM) with energy dispersive spectroscopy (EDS) was performed on both cathodically and anodically treated oxidized samples and on a bare sample after excessive cathodic exposure. Secondary (SE) and backscatter (BSE) electron imaging were used to accentuate morphological details and chemical contrast, respectively. The samples tested and pertinent data are listed in table III.

General Response

Rapid equivalent decay is evident in the current response curves for two René N5 samples at cathodic (–2.0 V) and anodic (2.0 V) polarizations (fig. 18) obtained for each leg by simply switching the output leads. The relative decay kinetics are also shown as normalized curves in figure 19. Here, similar response is observed for the three preoxidized samples, falling to about 25 to 40 percent of the initial currents after a few minutes. The as-polished unoxidized sample may take longer to build up concentration polarization effects because of the larger exposed metal surface areas.

Therefore, to map the current/voltage characteristic response (cf. voltammogram), the current after a standard 1 to 2 minute decay period was plotted, as were longer term exposures at a constant voltage. The solid line (fig. 20) plots behavior of the as-polished N5 coupon, whereas the data points show the behavior of the coupons pre-oxidized for 1000 1-hr cycles at 1150 °C. Samples labeled (H_2) had been prepared by hydrogen annealing in 5%H_2/Ar at 1150 °C for 100 hr; whereas samples designated by (A.R.) had been oxidized in the as-received condition. Severe bubbling at the working electrodes and excessive (100 mA) currents were noted above 1.3 V or below –2.0 V. This indicated substantial overvoltages for

the generation of O_2 or H_2 gas, respectively, at the working sample electrode. This compares with similar transitions at 1.0 and –0.5 V for bare N5 calibrated against a Ag/AgCl (KCl saturated) standard electrode (fig. 21), known to possess an equilibrium potential of (+0.197 V) on the hydrogen scale. Between these extremes the currents were much smaller (<2.5 mA) and the processes much more controlled.

The macrographs in figure 20 show that, at 2.0 V, anodic dissolution and undercutting of intact oxide occurred. At 0.0 V, holding for 1-hr produced no visible loss of material, whereas, after the same amount of time at –2.0 V, nearly the entire scale was stripped from the same sample, i.e., cathodic de-scaling. This sample had been hydrogen annealed and exhibited excellent scale adhesion, as previously shown in figure 9. A second sample subjected to cathodic –2.0 V potential is shown in figure 22 to be seriously stripped of scale within the first 10 min, followed by lesser amounts at 20 and 60 min. Finally, the unoxidized, as-polished sample was charged down to –3.0 V at 95 mA and exhibited blistering and cracking of the surface due to excessive hydrogen charging.

Microstructure

These features are shown in more detail in the SEM/SEI/BSE micrographs of figures 23 to 25. Anodic polarization at 2.0 V accentuated the dendritic structure of the alloy, showing considerable removal of metallic material, while retaining large areas of scale (fig. 23). Etched regions often alternated with chemically polished interdendritic features and microcracked layers. Only limited regions of new interfacial spalling existed, shown as unaltered oxide imprints in the metal.

In contrast, cathodic de-scaling at –2.0 V revealed in SEM/BSE imaging that the vast majority of the sample surface was bare metal having imprints of the oxide grains, as shown in the inset (fig. 24). Generally, only small entrained particles of Al_2O_3 scale remained, exhibiting both transgranular and intergranular fracture. Ta-rich particles, identified as TaC by X-ray diffraction (XRD) and SEM/EDS, were also observed at the exposed metal interface. Finally, extruding growths of HfO_2, also identified by XRD scans, could be found above the outer surface of most intact Al_2O_3 plates. Micro-deposition of dispersed Pt particles was also observed, presumably due to electrochemical Pt transport from the positive Pt wire to the negative René N5 electrode.

Finally, cathodic hydrogen over-charging the bare René N5+Y sample at –3.0 V is seen to cause surface failure with no applied stress (fig. 25). High hydrogen contents resulted in microcracking, delamination, and a disruption of the alloy integrity at γ/γ' interfaces. Similar features were found on both the intact external surface as well as in the underlying layers, exposed by flaking and blistering. Since this treatment represents an extreme, it may not be exactly the same mechanism producing interfacial failure at –2.0 V.

Weight Change

The samples were also monitored by weight change periodically throughout the electrolytic treatments (fig. 26). The sample polarized at 1.3 V showed very little weight loss of <0.25 mg/cm^2 and very low currents of <1.0 mA. Anodic polarization at 2.0 V, however, produced a continuous and severe weight loss of >8 mg/cm^2 with high currents of 110 mA. Additional weight loss occurred by removing a sooty corrosion product by ultrasonic cleaning. Cathodic polarization at –2.0 V produced massive scale delamination, most evident after only 10 min, but at low currents <1.0 mA. By contrast, once the scale was removed, little further weight loss was observed. It is interesting to point out that the more adherent hydrogen annealed sample actually produced more weight loss than the corresponding as-received sample. This may be due to the larger original amount of intact scale available for cathodic de-scaling.

The differences between anodic and cathodic weight change behavior can be further accentuated by mapping the rate of weight loss versus imposed current. For electrochemical dissolution, weight loss rate was reasonably commensurate with current for the anodic tests, performed at 1.3 or ramped to 2.0 V (fig. 26). In contrast, the cathodic tests performed at –2.0 V produced high initial weight losses. These subsided completely because very little spallation was possible after cathodie de-scaling (figs. 20 and 24).

Proposed Model

From the hydrogen embrittlement literature, it can be recalled that local electrochemical cells are possible at exposed oxide-metal interfaces in moist environments (ref. 24). Here H_2O is adsorbed on the exposed metal and dissociates to $(OH)^-$ by anodic oxidation of aluminum to Al^{+3}, forming $Al(OH)_3$ and H^+ on the active metal surface. This frees e^- to protected (passivated) areas, attracting and reducing H^+, which then diffuses into these negative (cathodic) regions under the scale. An analogous scheme has been chemically verified recently for the reaction of activated Al powders with water to form $Al(OH)_3$ bayerite accompanied by H_2 formation (refs. 28 and 29).

The underlying metal is also under biaxial tensile strain, analogous to hydrogen embrittlement in regions of triaxial tension ahead of the crack tip in bulk alloys. Any segregated impurities, primarily sulfur in this case, may serve as further, synergistic, interfacial embrittling agents (ref. 25). Sulfur is also known to retard the recombination of H^+ and its escape as H_2 (v).

Scale segments autocatalytically debond when the hydrogen concentration reaches a critical limit, reducing the interface toughness to where it can be overcome by the stored strain energy in the scale. This feature derives from the observation that scales directionally 'unzip' as humid air is allowed localized access to an exposed interface, analogous to the often discontinuous crack growth process documented for classic hydrogen embrittlement (ref. 23). It is also proposed that the scale cracking and spallation process itself is near instantaneous (τ_{spall3}), previously requiring some finite time for water dissociation and hydrogen diffusion ($\tau_{incubate2}$), relegating the remaining scale to much longer residence times ($\tau_{intact1}$), or indefinite immunity (ref. 7).

Summary and Conclusions

Thermal expansion mismatch and interfacial sulfur activity remain the major factors defining primary Al_2O_3 scale spallation. However, moisture-induced delayed spallation is a secondary, but often dramatic, illustration of an additional mechanistic detail. Here interfacial hydrogen embrittlement resulting from ambient air was presented as the causative factor. Standard electrochemical hydrogen charging techniques were successfully used to abruptly strip a mature Al_2O_3 scale at the oxide-metal interface. This is in contrast to a more gradual alloy dissolution process occurring during anodic polarization. Finally, with no applied voltage, the 1N H_2SO_4 electrolyte alone produced no additional scale spallation or dissolution (within the precision of the experiment) as monitored by weight change, induced current, or microstructure.

Induced steady-state currents varied sigmoidally with applied potential, achieving high negative values up to –95 mA, proportional to cathodic voltages <–2.0 V (–0.5 $V_{Ag/gCl}$), and high positive values up to 110 mA proportional to anodic voltages >1.3 V (1.0 $V_{Ag/AgCl}$). However, a nearly flat plateau of low current, <1 mA, existed in between these limits. Interfacial spallation and substantial initial weight losses of 2.7 mg/cm^2 first occurred at the low currents of the cathodic knee, where H^+ is produced at the cathodically polarized sample from electrolysis.

Thus, these experiments highlight the detrimental effects of hydrogen charging on alumina scale adhesion. The symptoms are highly analogous to moisture-induced embrittlement mechanisms known to occur for bulk alloys containing aluminum. It is therefore reasonable to propose that hydrogen embrittlement may also be the root cause of moisture-induced delayed spallation of Al_2O_3 scales and ultimately desktop spallation of TBC's.

References

1. J.L. Smialek, "Adherent Al_2O_3 Scales Formed on Undoped NiCrAl Alloys," presented at the *N.L. Peterson Mem. Symp. Proc. on Oxidation of Metals and Associated Mass Transport*, Orlando, FL, October, 1986, M.A. Dayananda, S.J. Rothman, and W.E. King, eds., TMS Proceedings, Warrendale, PA, 297–313 (1987).
2. B.K. Tubbs and J.L. Smialek, "The Effect of Sulfur Removal on Scale Adhesion to PWA 1480," in *Corrosion and Particle Erosion of Materials at High Temperature*, V. Srinivasan, K. Vedula, eds., TMS, Warrendale, PA, 459–487 (1989).
3. J.L. Smialek, "Adherent Scales Produced on Uncoated Superalloys: Desulfurized René 142 and René N5," presented at The David L. Douglass Symposium on High Temperature Corrosion, Extended Abstracts, The Electrochemical Society, Miami, FL, October, Paper No. 525, 833–834 (1994).
4. J.L. Smialek, D.T. Jayne, J.C. Schaeffer, and W.H. Murphy, "Effects of hydrogen annealing, sulfur segregation and diffusion on the cyclic oxidation resistance of superalloys: a review," Thin Solid Films, 253, 285–292 (1994).
5. J.L. Smialek: "Toward Optimum Scale and TBC Adhesion on Single Crystal Superalloys," High Temperature Corrosion and Materials Chemistry, E.J. Opila, P.Y. Hou, D. Shores, M. McNallan, and R. Oltra, eds., The Electrochemical Society Proceedings, vol. 98–9, Pennington, NJ, 211–220 (1998).
6. J.L. Smialek and B.A. Pint, "Optimizing Scale Adhesion for Single Crystal Superalloys," *Mater. Sci. Forum*, 369–372, 459–66 (2001). (also NASA TM 2000-210362).
7. J.L. Smialek and G.N. Morscher, "Delayed alumina scale spallation on René N5+Y: moisture effects and acoustic emission," *Materials Science and Engineering: A*, 332 (1–2), 11–24 (2002).
8. J.L. Smialek, "Scale Adhesion, Sulfur Content, and TBC Failure on Single Crystal Superalloys," in Ceramic Engineering and Science Proceedings, 23, [4], 485–495 (2002).
9. D.R. Sigler, "Adherence Behavior of Oxide Grown in Air and Synthetic Exhaust Gas on Fe-Cr-Al Alloys Containing Strong Sulfide-Forming Elements: Ca, Mg, Y, Ce, La, Ti, Zr," Oxidation of Metals, 40, 555–583 (1993).
10. M.A. Smith, W.E. Frazier, and B.A. Pregger, "Effect of sulfur on the cyclic oxidation behavior of a single crystalline, nickel-base superalloy," Materials Science and Engineering, A203, 388–398 (1995).
11. R. Janakiraman, G.H. Meier, and F.S. Pettit, "The Effect of Water Vapor on the Oxidation of Alloys that Develop Alumina Scales for Protection," *Metall. and Mat. Trans*., 30A, 2905–2913 (1999).
12. V. Sergo and D.R. Clarke, "Observation of Subcritical Spall Propagation of a Thermal Barrier Coating," *J. American Ceramic Society*, 81 [12] 142–161 (1998).
13. V. Tolpygo and D.R. Clarke, "Spalling failure of α-alumina films grown by oxidation: Parts I and II," Mater. Sci. Eng., A278, 142–161 (2000).
14. D. Renusch, H. Eschler, and M. Schutze, "Progress in life time modeling of APS-TBC," *Mat. High Temp*., 21, 65–76 (2004).
15. H.E. Zschau, M. Dietrich, D. Renusch, M. Schutze, J. Meijer, H.W. Becker, "Detection of Hydrogen in Hidden and Spalled Layers of Turbine Blade Coatings," *Nuclear Instruments and Methods B*, in press (2005).
16. A.K. Kuruvilla and N.S. Stoloff, Scripta Metall., 19, 83–88 (1985).
17. C.T. Liu, E.H. Lee, and C.G. McKamey, "An Environmental Effect as the Major Cause for Room Temperature Embrittlement in FeAl," Scripta Metall., 23, 875–880 (1989).
18. C.T. Liu, "Ni_3Al Aluminide Alloys," in Structural Intermetallics, R. Darolia, et al., eds., TMS, Warrendale, PA, 365–377, (1993).
19. N.S. Stoloff, "Hydrogen and Moisture-Induced Embrittlement of Nickel and Iron Aluminides, in Hydrogen Effects in Materials," A.W. Thompson, N.R. Moody, eds., TMS, Warrendale, PA, 523–537 (1996).
20. C.T. Liu, J. Stringer, J.N. Mundy, L.L. Horton, P. Angelini, "Ordered intermetallic alloys: an assessment," Intermetallics, 5, 579–596 (1997).

21. J. Gayda, R.L. Dreshfield, and T.P. Gabb, "The Effect of Porosity and γ/γ' Eutectic Content on the Fatigue Behavior of Hydrogen Charged PWA 1480," Scripta Met. et Mat., 25, 2589–2594 (1991).
22. J. Gayda, T.P. Gabb, and R.L. Dreshfield, " The Effect of Hydrogen on the Low Cycle Fatigue Behavior of a Single Crystal Superalloy," in Hyddrogen Effects on Material Behavior, N.R. Moody, A.W. Thompson, eds., TMS, Warrendale, PA, 591–601 (1990).
23. A.R. Troiano, "The Role of Hydrogen and Other Interstitials in the Mechanical Behavior of Metals," 34th Edward De Mille Campbell Memorial Lecture, Chicago, Nov. 4, 1959, in ASM Transactions, 52, 54–80 (1960).
24. R.P. Wei and M. Gao, "Hydrogen Embrittlement and Environmentally Assisted Crack Growth," in Hydrogen Effects on Material Behavior, N.R. Moody, A.W. Thompson, eds., TMS, Warrendale, PA, 789–816 (1990).
25. R.H. Jones, "Hydrogen and Impurity-Induced Intergranular Crack Growth," in Hydrogen Effects on Material Behavior, N.R. Moody, A.W. Thompson, eds., TMS, Warrendale, PA, 817–843 (1990).
26. J.L. Smialek, "Effect of Moisture on Secondary Spallation of Alumina Scales on Y-doped René N5," presented at the TMS Symposium, Water Vapor Effects on the Oxidation of High Temperature Materials, Seattle, WA, P. Tortorelli, et al., chairs, Feb. 18–22, (2002).
27. J.L. Smialek, "Desk Top TBC Spallation and Interfacial Hydrogen Embrittlement of Alumina Scales," presented at the TMS Symposium, Superalloys and Coatings for High Temperature Applications, San Francisco, CA, Feb. 13–17, 2005.
28. Z.Y. Deng, Y.F. Liu, Y. Tanaka, J.H. Ye, and Y. Sakka, "Modification of Al Particle Surfaces by γ-Al_2O_3 and its Effect on the Corrosion Behavior of Al," J. Am. Ceram. Soc., 88, 977–979 (2005).
29. Z.Y. Deng, Y.F. Liu, Y. Tanaka, H.W. Zhang, J.H. Ye, and Y Kagawa, "Temperature Effect on Hydrogen Generation by the Reaction of γ-Al_2O_3- Modified Al Powder with distilled Water," J. Am. Ceram. Soc., 88, 2975–2977 (2005).

The nominal compositions of alloys to be discussed are listed in table I. They are generally cast nickel base superalloys with high Al and Ta contents, and moderate Cr levels. These elements are well known to be associated with maximum oxidation resistance of commercial superalloys. The reactive element Y is certainly effective in providing scale adhesion. However, Hf, which is also reactive and shows some beneficial effect, is not as effective.

TABLE I.—NOMINAL SUPERALLOY COMPOSITIONS AND PREVALENT SCALE COMPONENTS

(Ni-base, wt%)

Alloy	Co	Al	Cr	Ta	W	Mo	Re	Ti	Hf	Y
PWA 1480	5	**5.0**	10	12	4	0	0	1.5	0.0	0.0
PWA 1484	10	**5.6**	5	9	6	2	3	0.0	0.1	0.0
René 142	13	**6.2**	6	6	6	13	3.5	0.0	2.0	0.0
René N5	8	**6.2**	7	7	5	2	3	0.0	0.2	0–100 ppmw

Al_2O_3, $Ni(Al,Cr)_2O_4$, $CrTaO_4$, $NiTa_2O_6$, HfO_2, Cr_2O_3, NiO, TiO_2

(protective, neutral, and detrimental)

Some remarkable similarities between alloy embrittlement and scale spallation are listed in table II. First, it is well-known that sulfur segregation is responsible for many manifestations of intergranular temper embrittlement in steels, and it has been identified as the responsible interface contaminant resulting in the spallation of protective Al_2O_3 and Cr_2O_3 scales. Hydrogen embrittlement is also a classic topic of interest for many aqueous environment issues regarding high strength steels, nickel, titanium, and aluminum alloys. While cleavage may be produced in some cases, intergranular embrittlement and failure is a common characteristic. The hydrogen source can, in some cases (e.g., intermetallic compounds) be just the moisture in ambient air, such that dry oxygen or vacuum may result in more ductile behaviors. The present review of Al_2O_3 spallation caused by moisture and water immersion above is certainly consistent with this phenomenon.

Slow strain rate sensitivity and intermittent crack growth models, observed in some hydrogen embrittlement studies, are based on the time needed to diffuse hydrogen ahead of the crack tip. Room temperature or slightly above is observed to maximize embrittlement effects due to fast hydrogen diffusion at this temperature. However, at elevated temperature, the diffusion becomes so fast that the hydrogen escapes from the material. The delayed and intermittent spallation of oxidized alumina-formers, after removal from the dry environment of the furnace cooling chamber, is reminiscent of such phenomena. The state of triaxial tension is often presented as a requirement to attract and hold hydrogen in sufficient quantity to cause embrittlement. Similarly, the biaxial tension produced by thermal expansion mismatch with the scale and growth stresses in the scale presents an attractive stress condition for hydrogen at the metal side of the oxide-metal interface.

There have been enough theoretical studies of sulfur and hydrogen effects on metal-metal and Al_2O_3-metal interfaces to strongly suggest that both elements will cause interfacial weakening. Indeed, in the case of metal embrittlement a negative synergy has been observed, where a sulfur contaminated interface may be necessary to observe serious hydrogen effects. Thus it remains to be seen whether hydrogen driven into the oxide metal interface can produce spallation and whether a negative synergy also exists between a sulfur-weakened Al_2O_3-metal interface and hydrogen. It is useful to point out here that in a number of cases the susceptibility of scales to delayed, moisture-induced spallation appeared to be well-correlated with marginal adhesion and moderately sulfur contaminated interfaces. Therefore, in order to isolate hydrogen embrittlement from other moisture effects as the primary criterion for delayed scale spallation, standard electrochemical hydrogen charging techniques are employed.

An old adage can therefore be applied to the relative newcomer of impurity (sulfur) controlled scale adhesion/spallation theories, developed from about 1985 to the present. It builds upon similar intergranular phenomena that have been previously well-established from about 1951 to 1989. The proposed parallelisms follow Occam's Razor (from William of Occam, 1836), which provides "a scientific and philosophic rule that entities should not be multiplied unnecessarily…the simplest of competing theories be preferred to the more complex….that explanations of unknown phenomena be sought first in terms of known quantities."

TABLE II.—FEATURES OF HYDROGEN EMBRITTLEMENT IN BULK ALLOYS AND INTERMETALLICS ANALOGOUS TO THOSE OBSERVED OR PROPOSED FOR INTERFACIAL EMBRITTLEMENT OF ALUMINA SCALES

Common Condition	Alloy Fracture (1951–1989)	Scale Spallation (1985–2005)
Sulfur segregation	Intergranular embrittlement	√ Interfacial weakening
Moisture effects Hydrogen diffusion Tensile stress state	Intergranular and cleavage Delayed failure at room temperature Intermittent crack growth	√ Interfacial weakening √ Delayed room temperature failure √ Intermittent spallation
Theoretical strength	H, S decrease M-M bond	√ H, S decrease M-Al_2O_3bond
H+S segregation	Negative synergy	? **Negative synergy**
Cathodic charging	H-embrittlement	? **Interfacial de-scaling**

Occam's Razor: keep it simple and draw from known experience

The René N5 samples and pertinent oxidation, immersion, and electrochemical treatment data are summarized in table III. H_2 condition refers to hydrogen annealing in 5%H_2/Ar at 1250 °C for 100 hr. Y and S content was determined by GDMS. Net weight change is after 1000 1-hr cycles at 1150 °C, and H_2O weight is the additional spallation due to immersion. Current response and weight losses are listed for about 1 hr at the applied voltage in 1 N H_2SO_4, with data for selected secondary treatments. It is seen that the hydrogen annealed samples formed comparatively more adherent scales (even though no desulfurization occurred). Anodic polarization resulted in little current or weight loss at 1.3 V, but high levels of each at 2.0 V, shown to be alloy dissolution. Immersion in H_2SO_4 at 0.0 V resulted in very little change, but subsequent cathodic polarization at –2.0 V produced substantial 1.3 to 2.7 mg/cm^2 losses at currents less than –0.5 mA, primarily due to de-scaling. Finally, an unoxidized sample lost 4 mg/cm^2 by anodic 1.8 V dissolution, followed by 0.5 mg/cm^2 by cathodic –3.0 V hydrogen overcharging and blistering.

TABLE III.—RENÉ N5 CYCLIC OXIDATION, WATER IMMERSION, AND H_2SO_4 POLARIZATION (mg/cm^2 weight change)

Sample	Condition	Y, ppmw	S, ppmw	1000 hr	ΔW_{H20}	V	*i*, mA	ΔW_1	ΔW_{1+2}	Second treatment
48–1	H_2	20	7.0	0.638	–0.107	1.3	0.70	–0.258	–0.347	2 min at –2.0 V
48–2	A.R.	20	5.2	–0.972	–0.415	2.0	112.0	–5.462	–8.317	Ultrasonic de-sooting
67–1	H_2	80	5.5	0.932	–0.068	0.0	0.00	–0.041		
						–2.0	–0.37	–2.730		
67–2	A.R.	80	4.9	–1.162	–0.122	–2.0	–0.43	–1.315		
N5–0	A.R.	0.3	2.6	-----	-----	1.8	3.1	–3.983		
						–3.0	–95	–0.541		

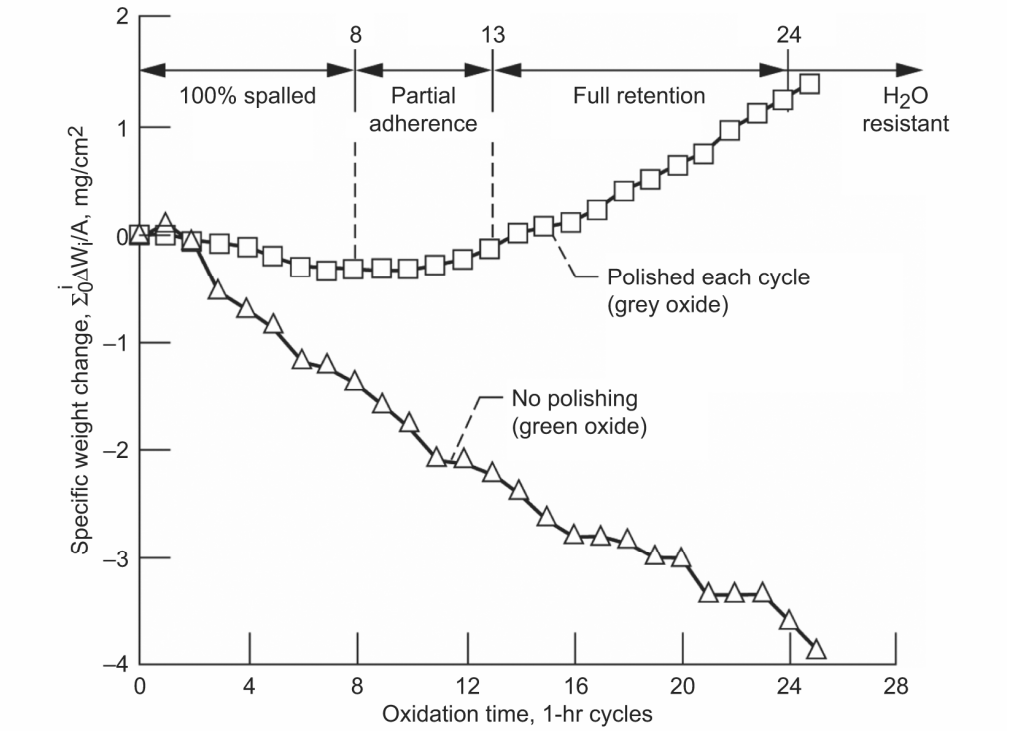

Figure 1.—Adherent Al_2O_3 behavior induced in undoped NiCrAl during 1120 °C cyclic oxidation. Cumulative weight change measured after 1 hour oxidation, then polished off and repeated, as compared to control (unpolished) sample, (from ref. 1).

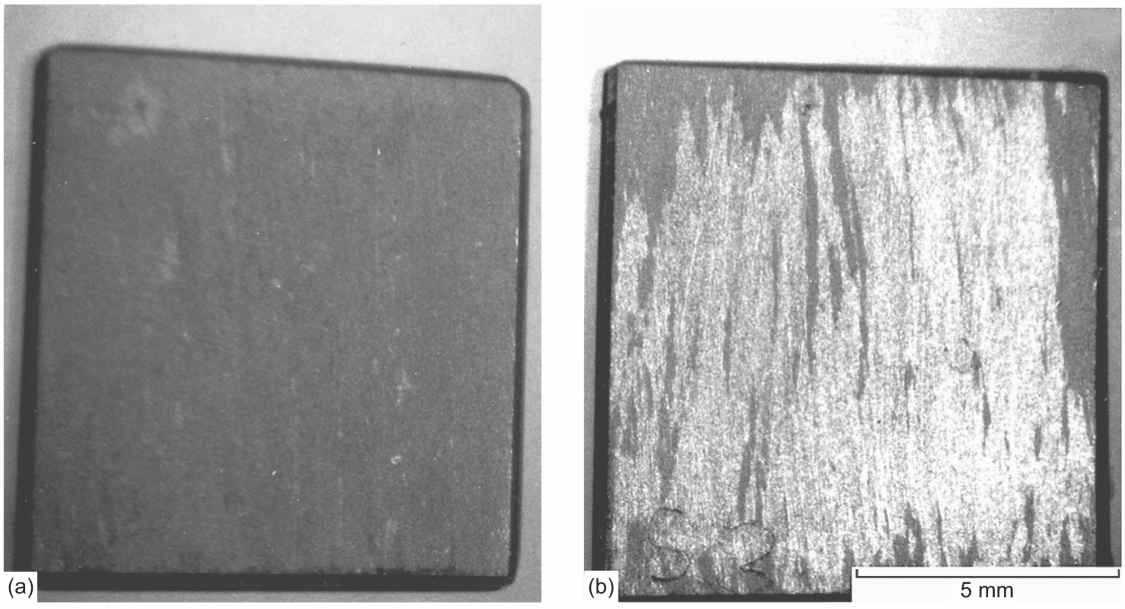

Figure 2.—Retained Al_2O_3 scale. (a) After 15 oxidation/polishing cycles, then (b) removed by water immersion. (Undoped NiCrAl oxidized at 1120 °C in 1-hr cycles, from ref. 1).

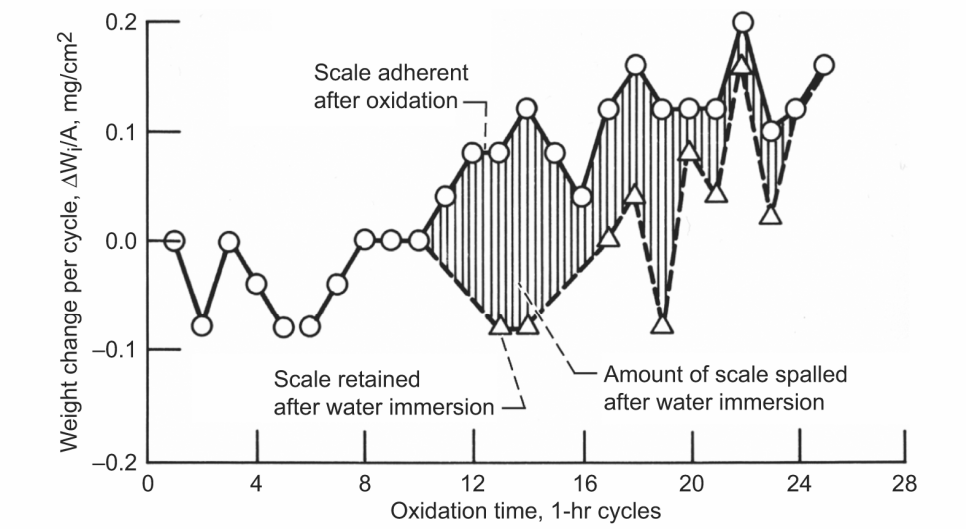

Figure 3.—Amount of additional spallation induced by water immersion (shaded area) for each oxidation/polishing cycle. (Undoped NiCrAl oxidized at 1120 °C in 1-hr cycles, from ref. 1).

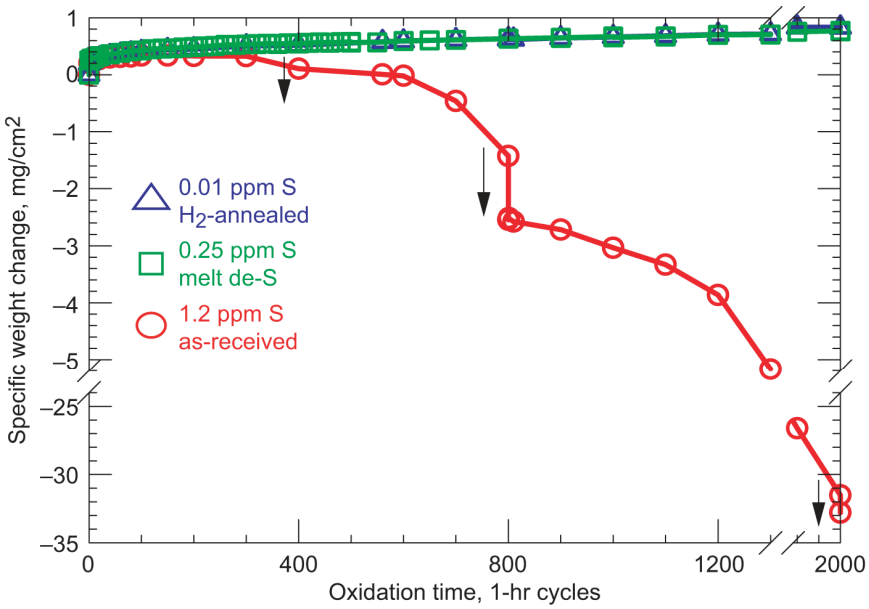

Figure 4.—Adherent cyclic oxidation behavior at 1100 °C produced for low sulfur PWA 1484 samples: conventional 1.2 ppmw S, melt desulfurized to 0.25 ppmw S, and hydrogen annealed to 0.01 ppmw S. Additional spallation due to immersion indicated by vertical arrows. (from ref. 5 and 8).

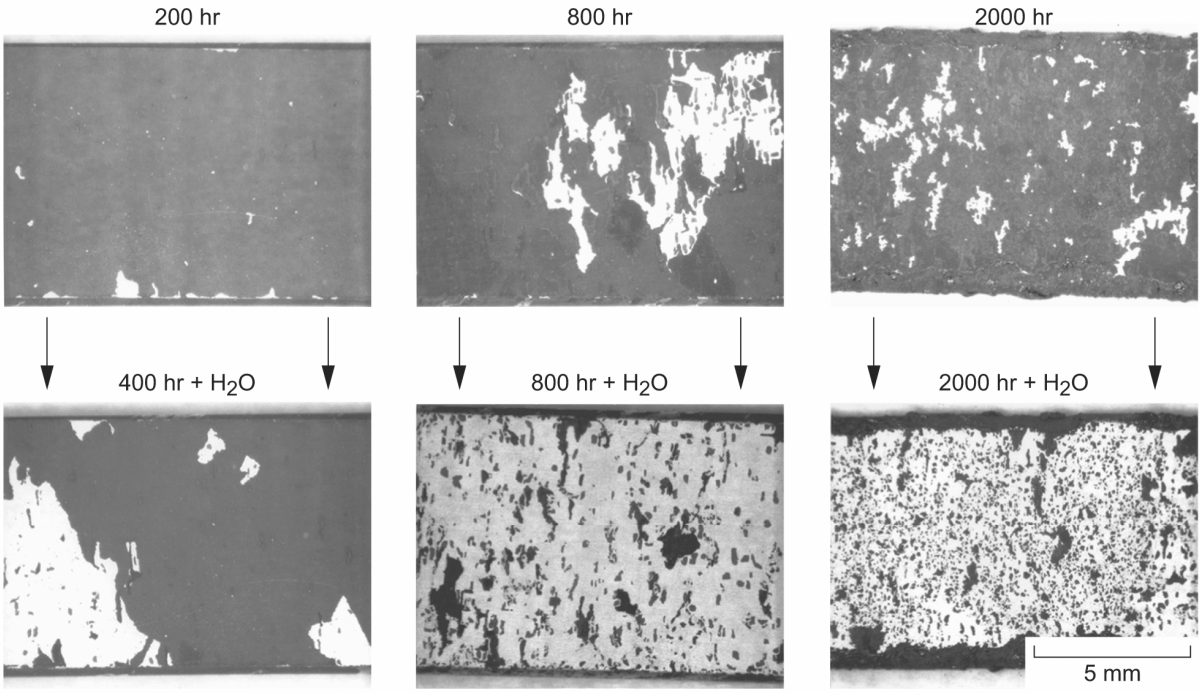

(a)

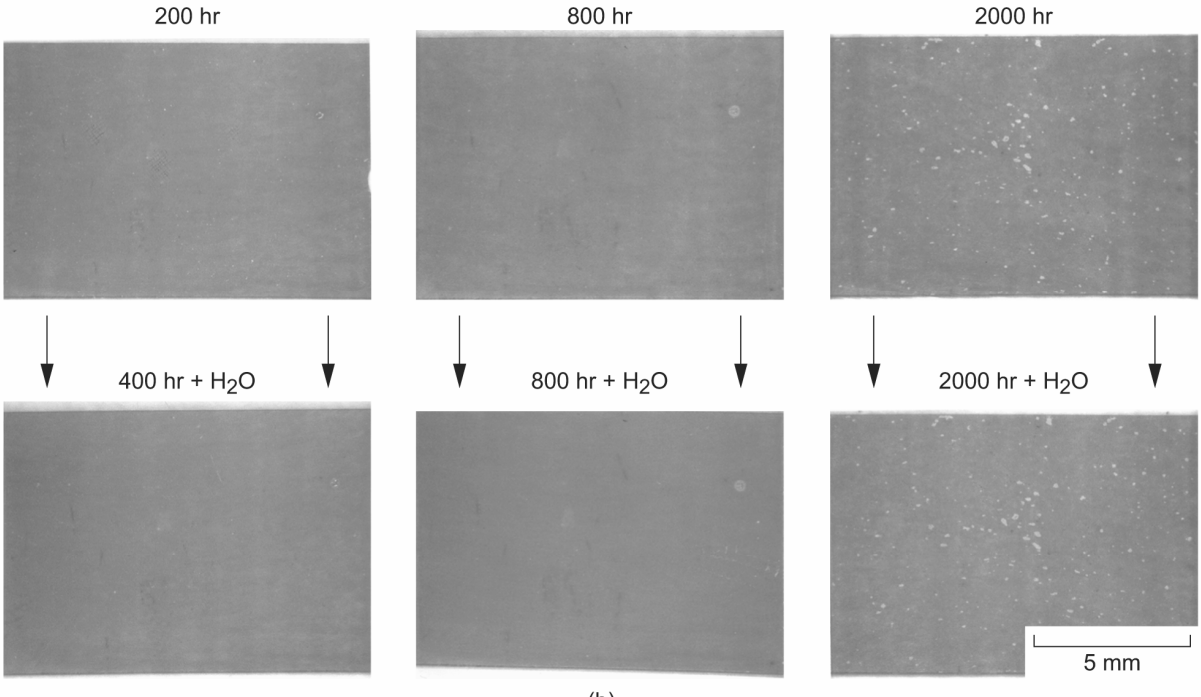

(b)

Figure 5.—Effect of water immersion on interfacial scale spallation for PWA 1484, cyclically oxidized at 1100 °C. (a) Major effect for as-received sample at 1.2 ppmw S; (b) No effect on extremely adherent behavior for hydrogen annealed sample at 0.01 ppmw S.

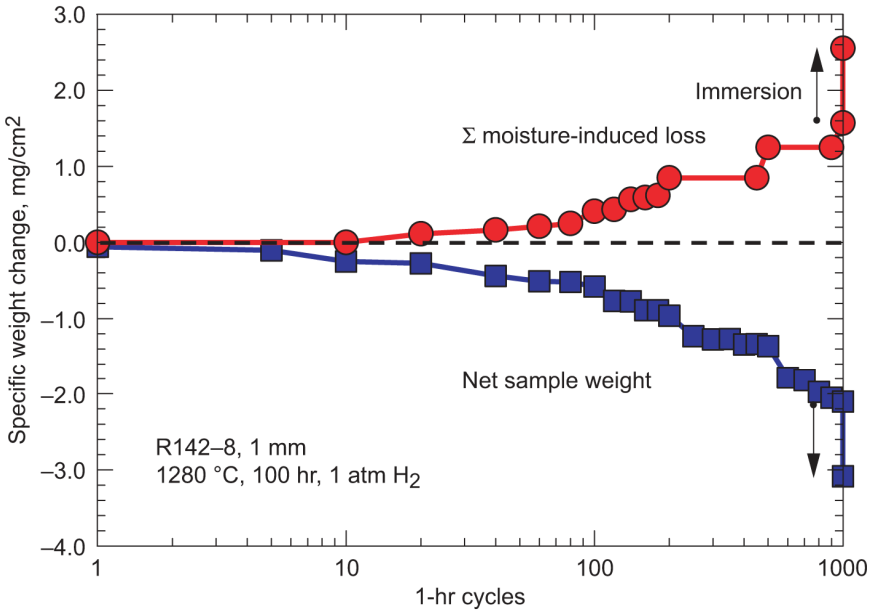

Figure 6.—Amount of additional spallation induced by moist breath exposure (upper curve) for René 142 oxidized at 1150 °C in 1-hr cycles. (Sample 142–6, 1 mm thick, annealed in 1 atm. H_2 at 1280 °C for 100 hr; vertical arrows show water immersion effect at 1000 hr).

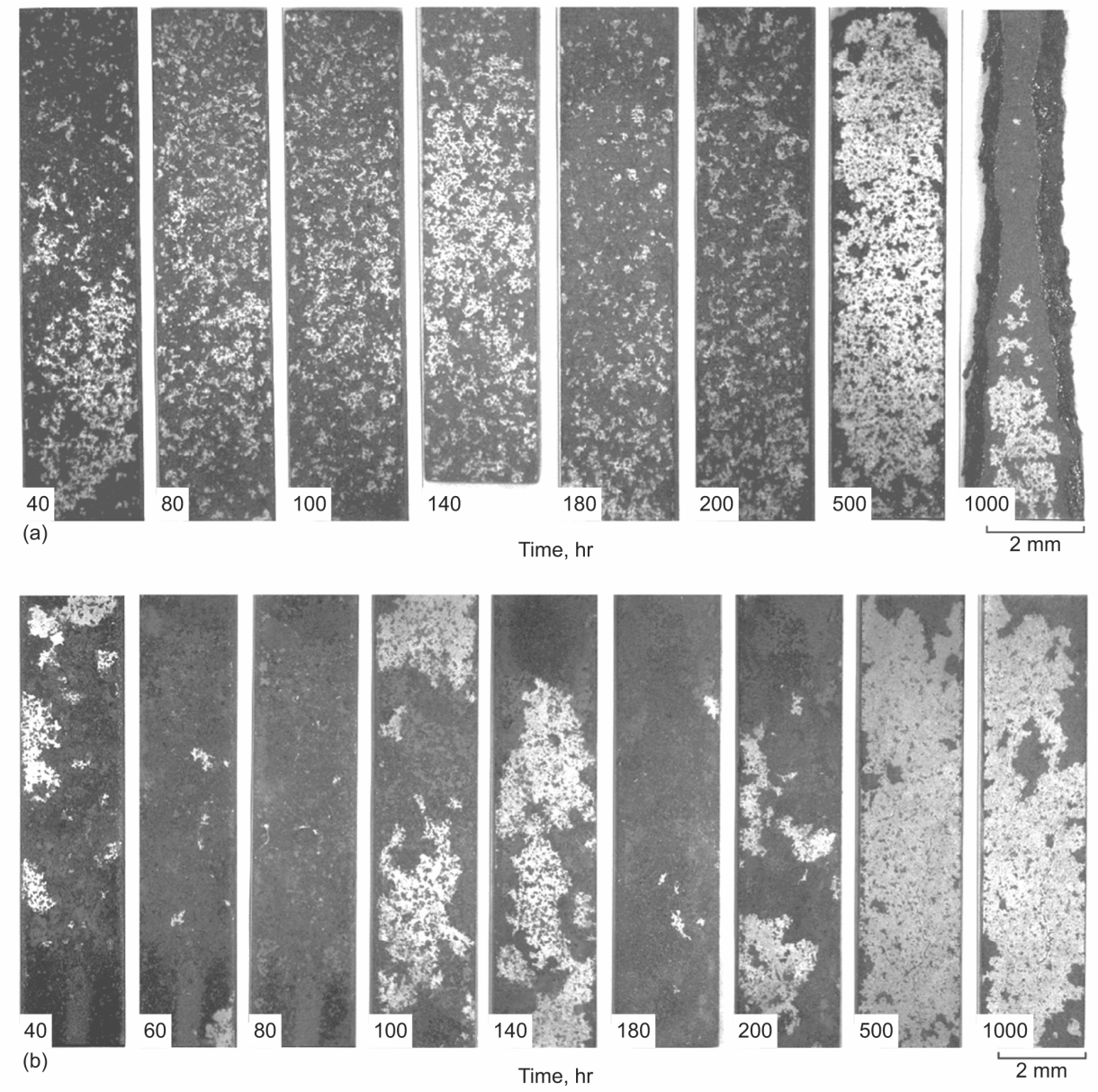

Figure 7.—Interfacial spallation induced by moist breath for René 142 oxidized at 1150 °C in 1-hr cycles: (a) As-received sample 142–6, 6.1 ppmw S, 1 mm thick; (b) Sample 142–8, annealed in 1 atm. H_2 at 1280 °C for 100 hr, 0.3 ppmw S, 1 mm thick.

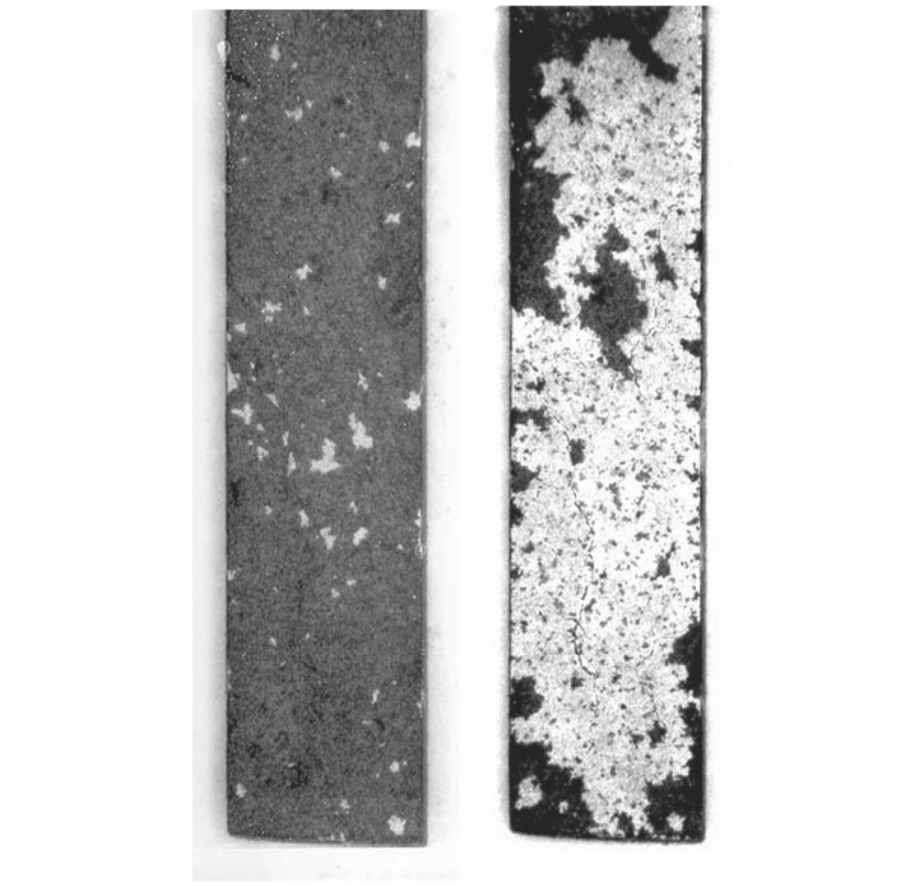

As-cooled After immersion

Figure 8.—The effect of water immersion on interfacial scale spallation after 1000 cycles at 1150 °C. (René 142–8, annealed in 1 atm. H_2 at 1280 °C for 100 hr, 0.3 ppmw S).

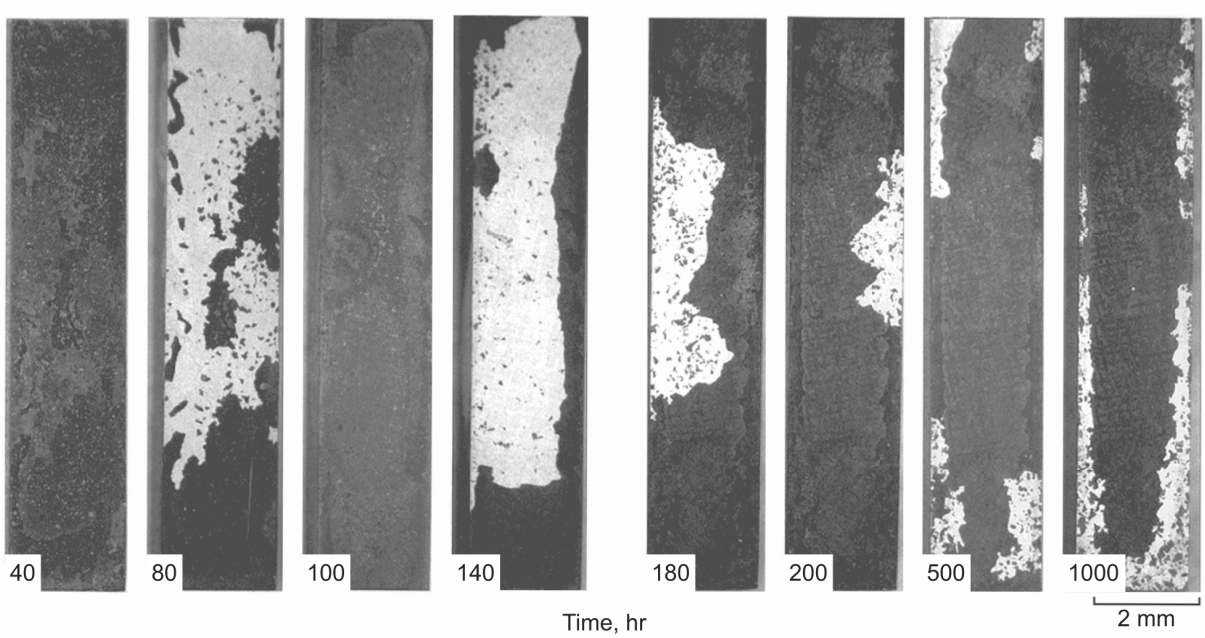

Figure 9.—Interfacial spallation induced by moist breath for René N5 oxidized at 1150 °C in 1-hr cycles. (Sample N5–2, annealed in 1 atm. H_2 at 1280 °C for 100 hr, ~100 ppmw Y-doped, 3.7 ppmw S, 3 mm thick).

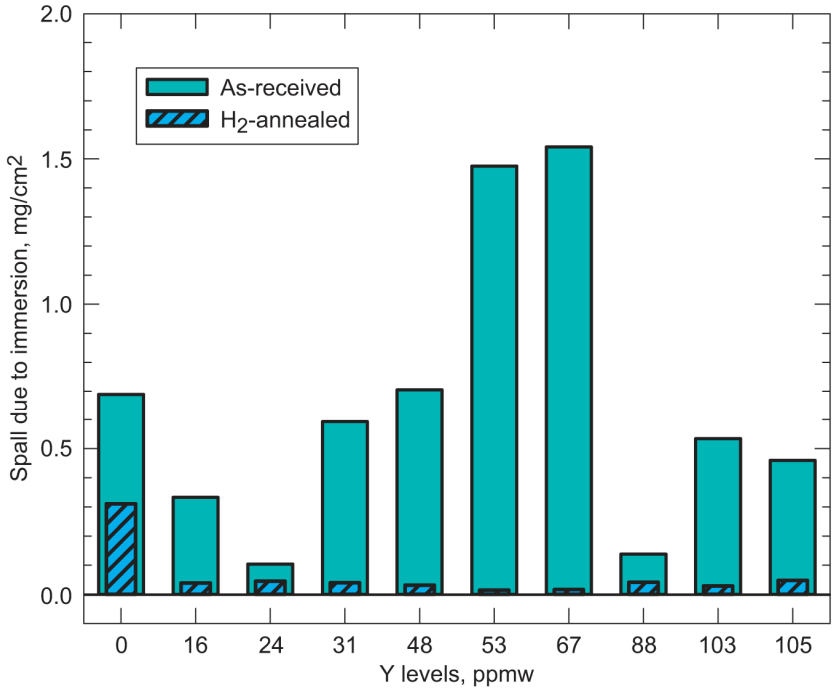

Figure 10.—Effect of water immersion on the amount of additional spallation for René N5±Y after 500 1-hr cycles at 1150 °C: appreciable for as-received and minimal for hydrogen annealed samples (5% H_2/Ar at 1250 °C for 100 hr, from ref. 6 and, 7).

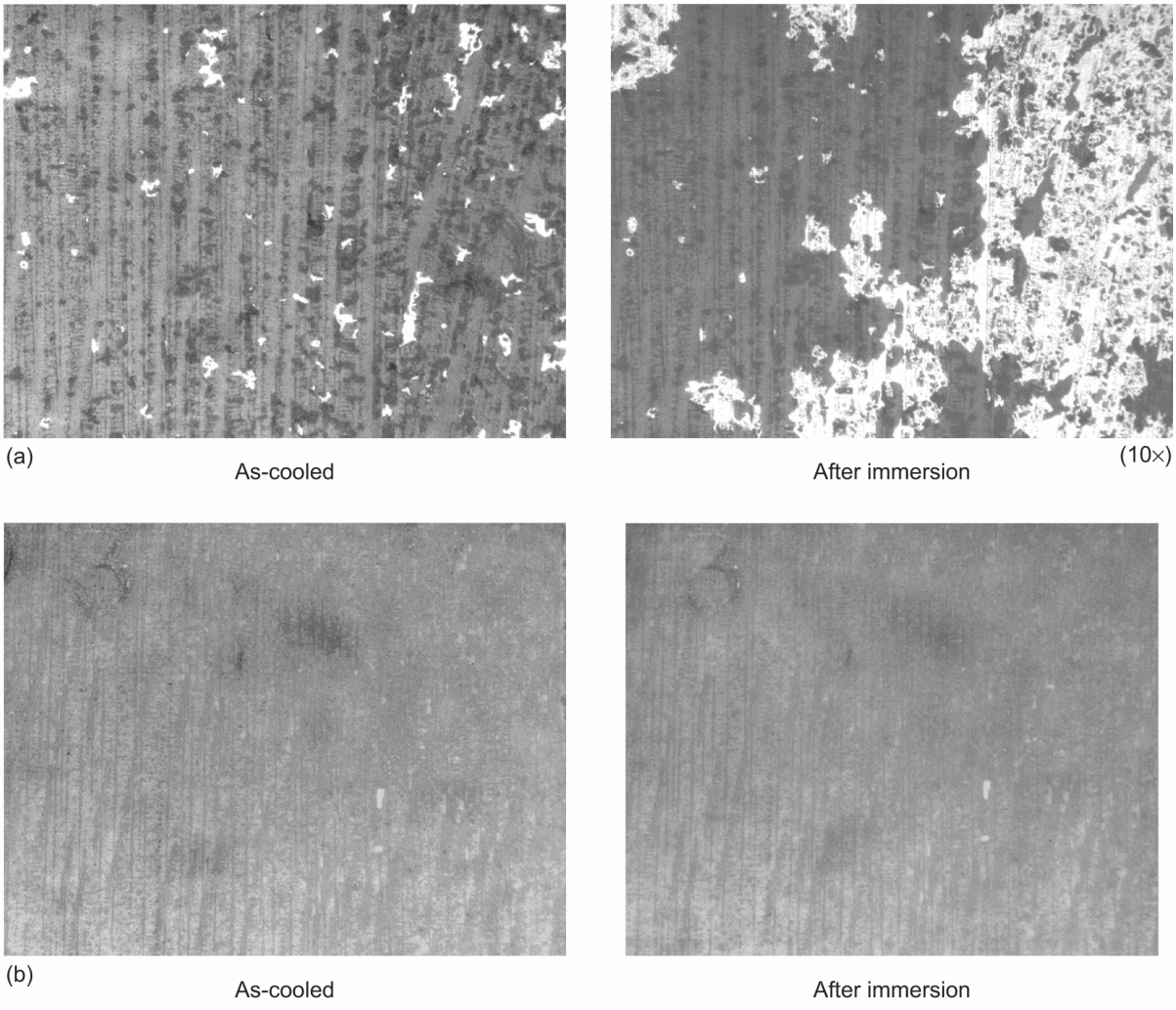

Figure 11.—Effect of water immersion on interfacial spallation for René N5+103Y after 500 1-hr cycles at 1150 °C: appreciable for (a) as-received and minimal for (b) hydrogen annealed (5% H_2/Ar at 1250 °C for 100 hr) samples, corresponding to figure 10.

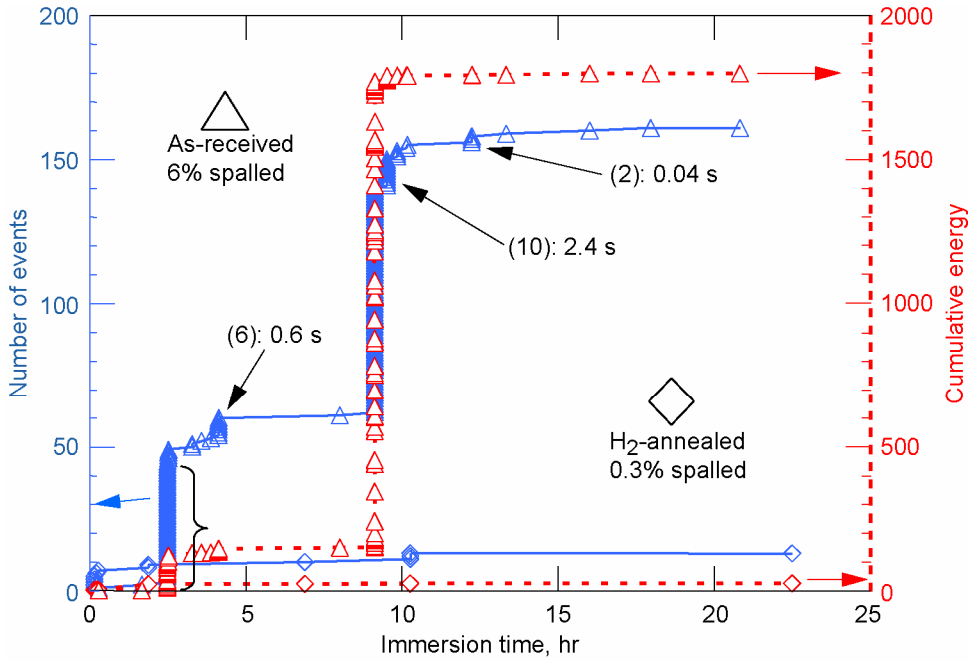

Figure 12.—Delayed failure and acoustic emission response of René N5 in long term water immersion of as-received (triangles) and hydrogen annealed (diamonds, 5% H_2/Ar at 1250 °C for 100 hr) samples. (Doped with 100 ppmw Y and oxidized at 1150 °C for 1000 1-hr cycles, from ref. 7).

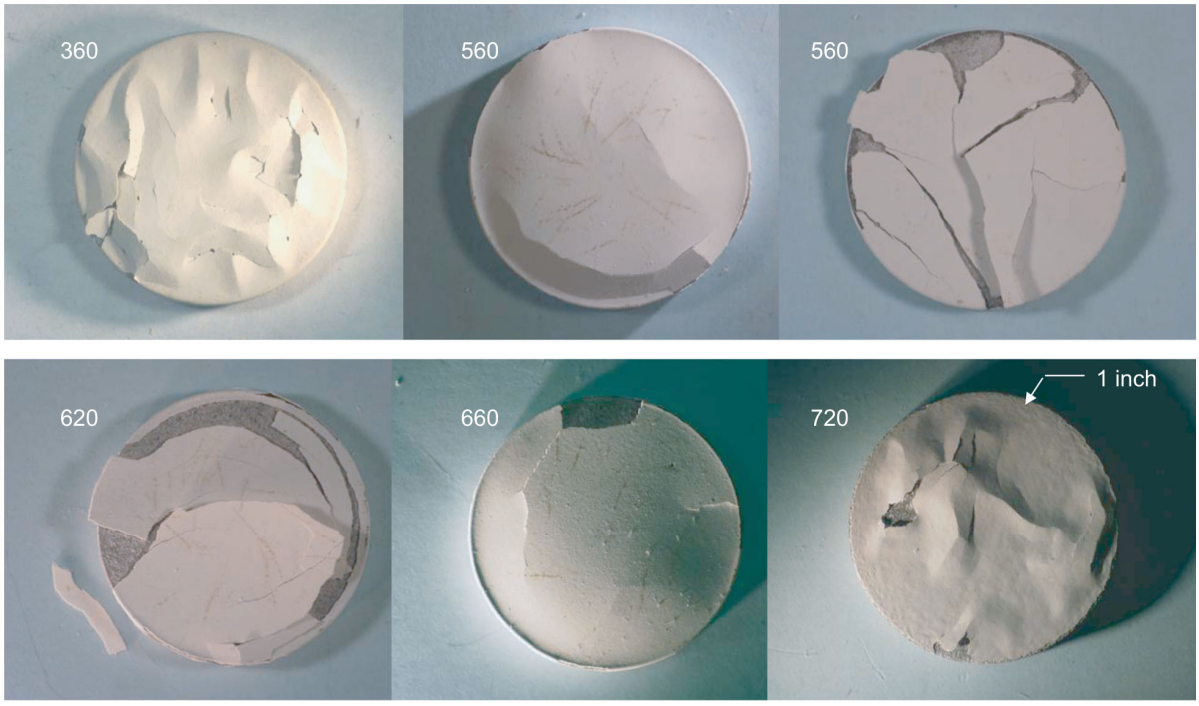

Figure 13.—Massive EB-PVD TBC buckling and cracking failures after cyclic oxidation, observed as desktop spallation delayed after cooldown. Cycles to failure noted. (Modified ZrO_2 coatings, with Ni(Pt)Al bond coat on René N5, oxidized at 1135 °C with 45 min cycles).

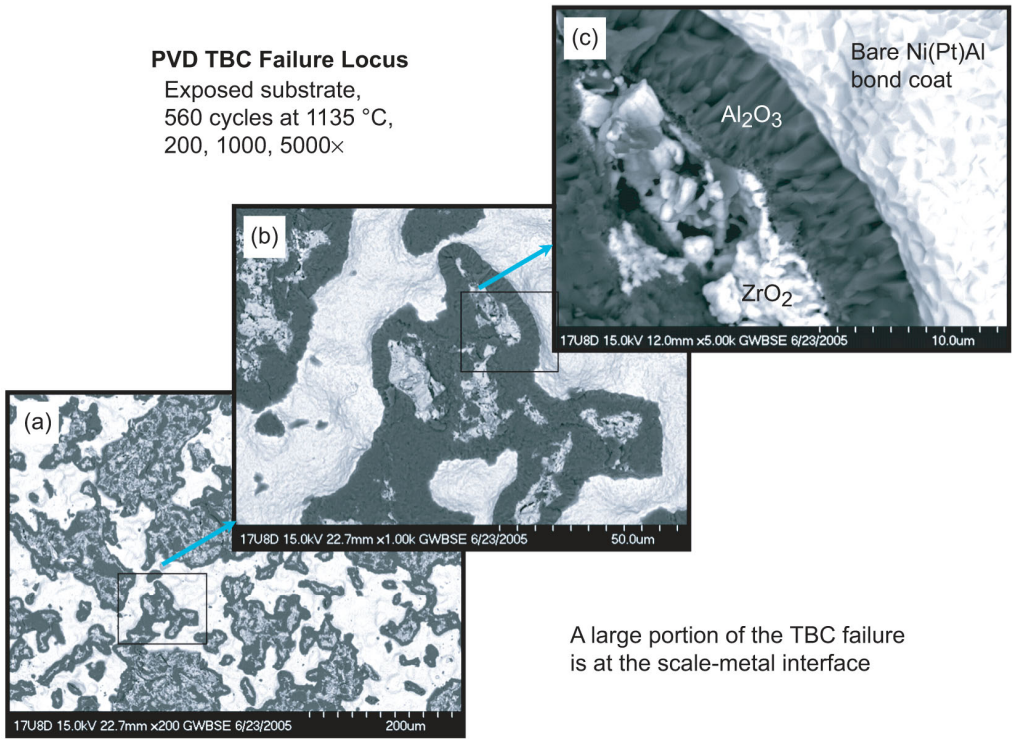

Figure 14.—Backscatter electron images showing (a) islands of retained scale (dark) in a sea of exposed metal (bright); (b) dispersions of TBC (light) attached within these islands, and (c) columnar Al_2O_3 intrusion, growing perpendicular to the Ni(Pt)Al bondcoat, with oxide grain imprints in exposed metal. Regions identified by SEM/EDS as Al(O), Zr(Y), and Ni(Pt, Al, Ta, Cr) rich areas for α•Al_2O_3, t′-ZrO_2, and Ni(Al) identified by XRD of the entire region.

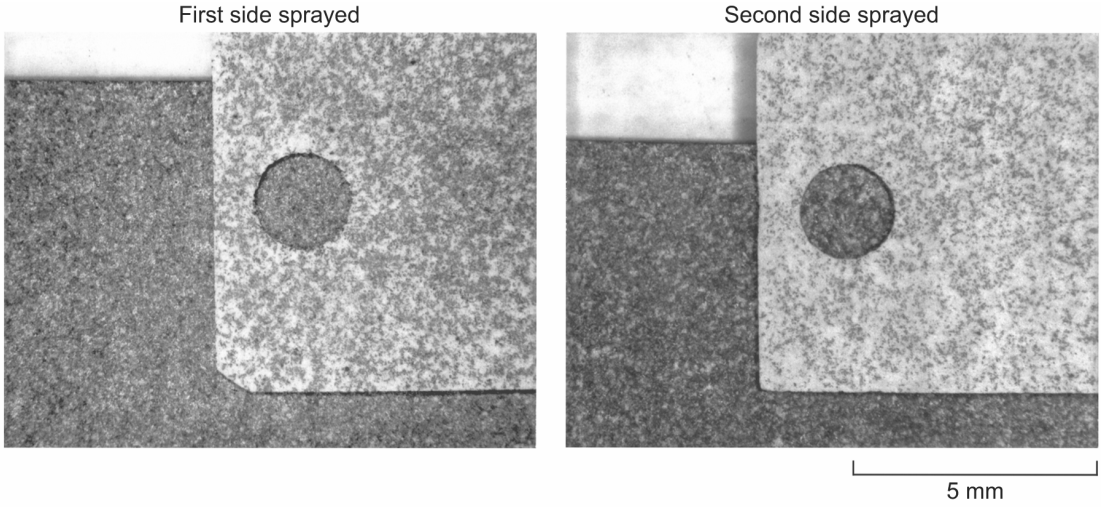

Figure 15.—Fully delaminated desktop spallation of plasma sprayed 8YSZ on grit blasted PWA 1484 containing 1.2 ppmw S. (No bond coat, 250 μm thick, oxidized at 1100 °C for 200 1-hr cycles).

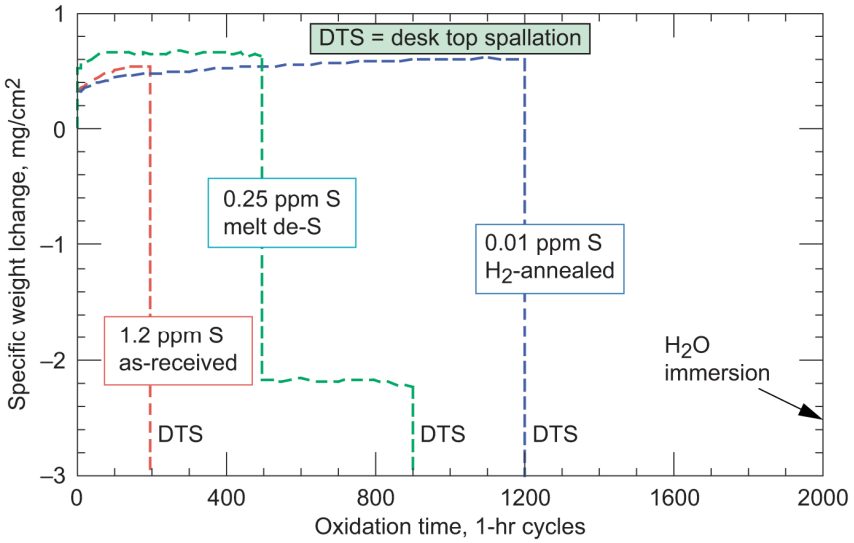

Figure 16.—The effect of sulfur content on the cyclic weight change and failure times for TBC's on PWA 1484. (No bond coat, 250 μm thick, oxidized at 1100 °C using 1-hr cycles). Vertical drops indicate coating spallation, desktop spallation, and water immersion failures.

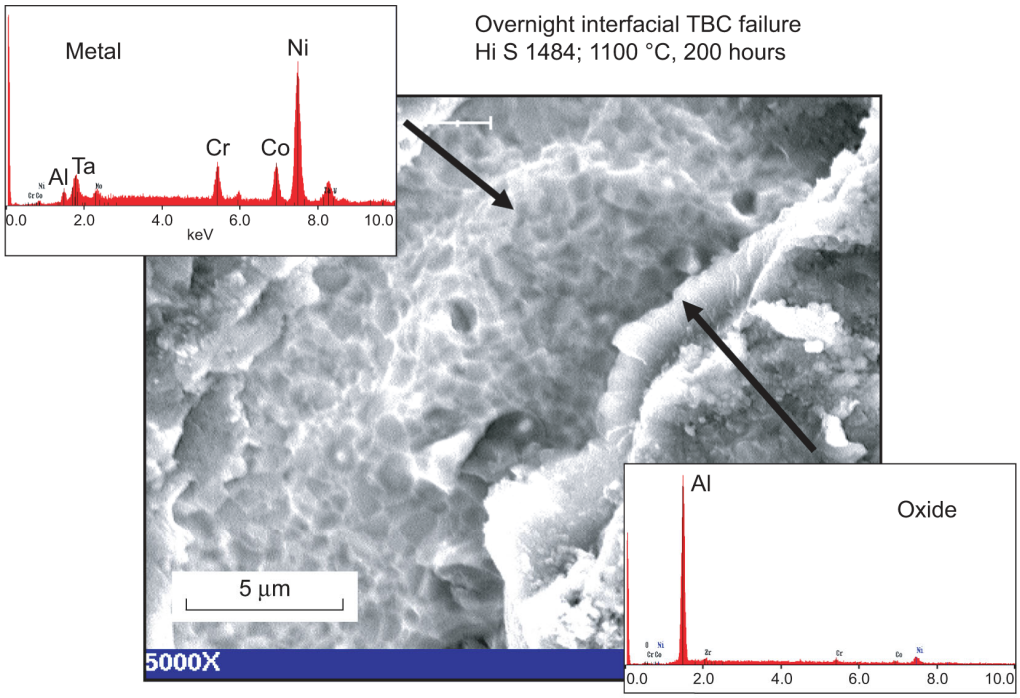

Figure 17.—Oxide imprints in metal and inner Al_2O_3 scale identified at the interfacial failure sites in PWA 1484. (1.2 ppmw S, no bond coat, 250 μm thick, oxidized at 1100 °C for 200 1-hr cycles, from figure 15).

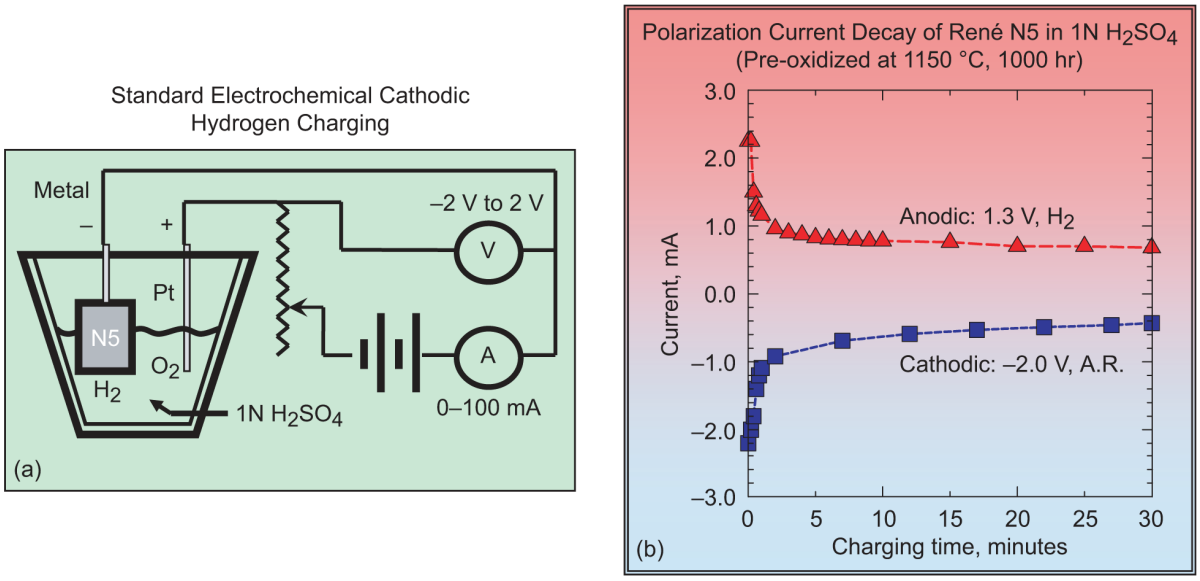

Figure 18.—Electrochemical hydrogen charging of pre-oxidized René N5 samples. (a) Cell schematic. (b) Typical current decay curves for anodic and cathodic polarizations in 1N H_2SO_4 electrolyte at room temperature. (1150 °C, 1000 1-hr cycles, from the studies in ref. 6 and 7).

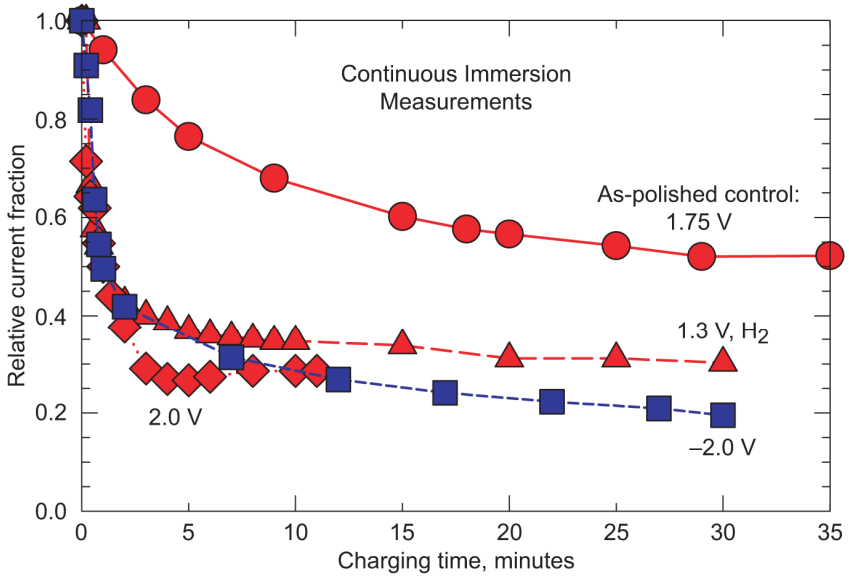

Figure 19.—Normalized current decay curves for pre-oxidized and bare René N5 coupons in 1N H_2SO_4.

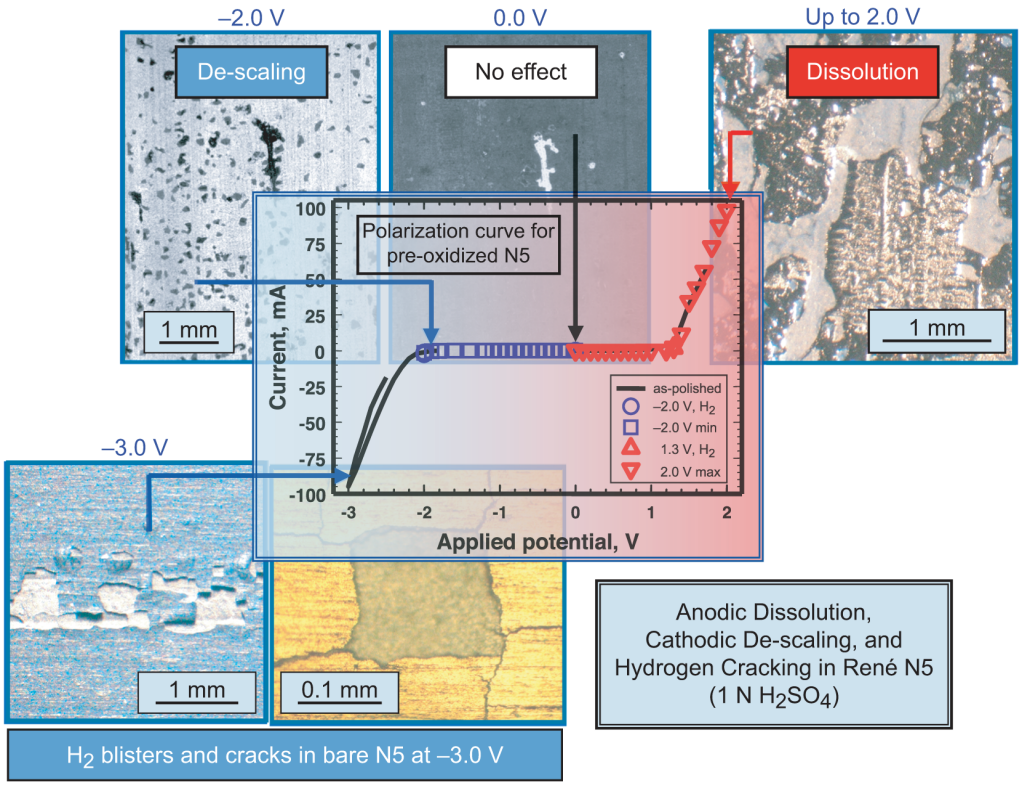

Figure 20.—Current response at 0.1 V stepped applied voltages (voltammogram), superimposed on macrographs illustrating: anodic dissolution of the alloy, null results at zero voltage, interfacial de-scaling at mild cathodic currents, and severe alloy blistering for extreme cathodic currents. (René N5+Y oxidized at 1150 °C, 1000 1-hr cycles, from the studies in ref. 6 and 7).

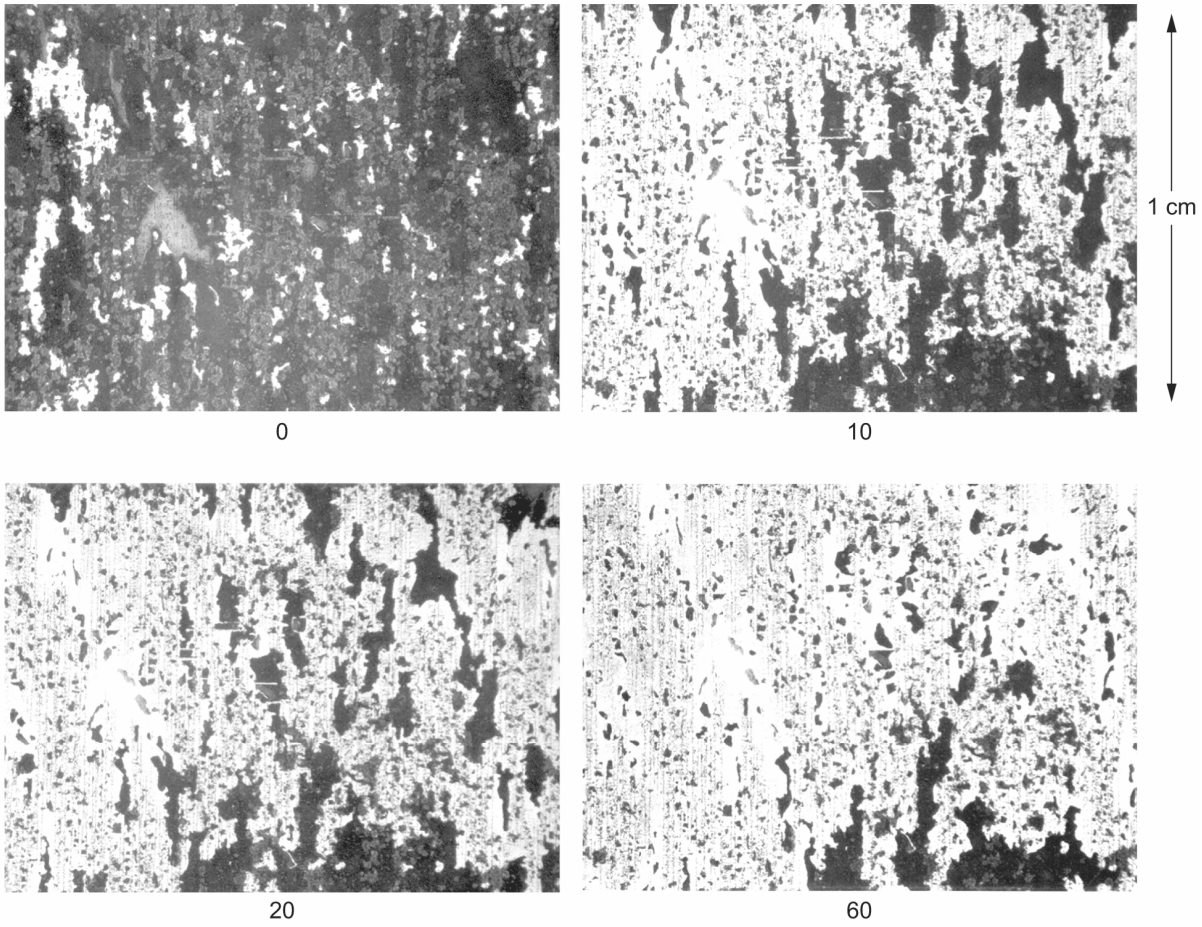

Figure 21.—Macrographs obtained after 0, 10, 20, and 60 min of cathodic charging at –2.0 V showing rapid interfacial de-scaling of René N5+80Y. (As-received, pre-oxidized at 1150 °C for 1000 hr).

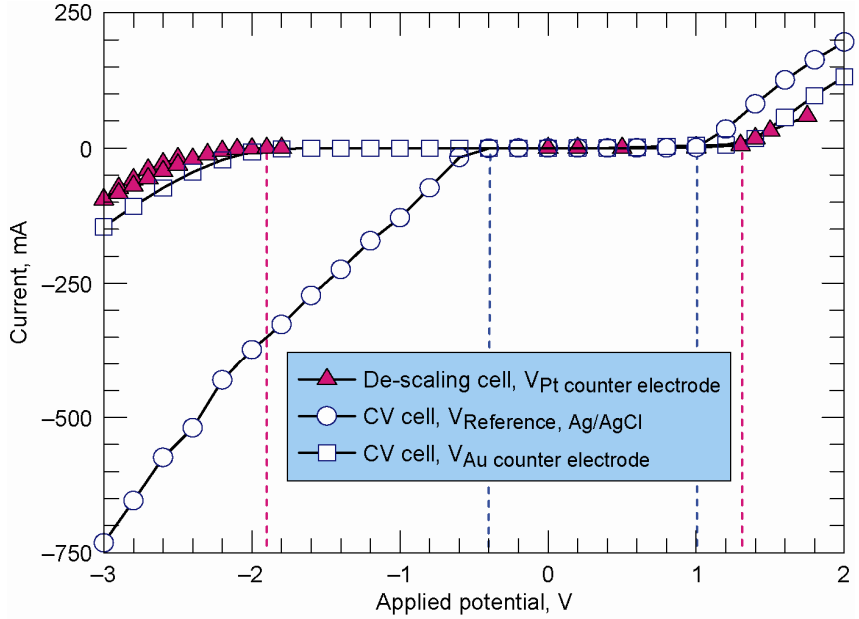

Figure 22.—Voltammograms obtained in a cell with Pt counter electrode compared to that obtained using an Ag/AgCl reference electrode, showing anodic/cathodic transitions at ~1.3/–1.9 V and 1.0/–0.4 V, respectively, in 1N H_2SO_4.

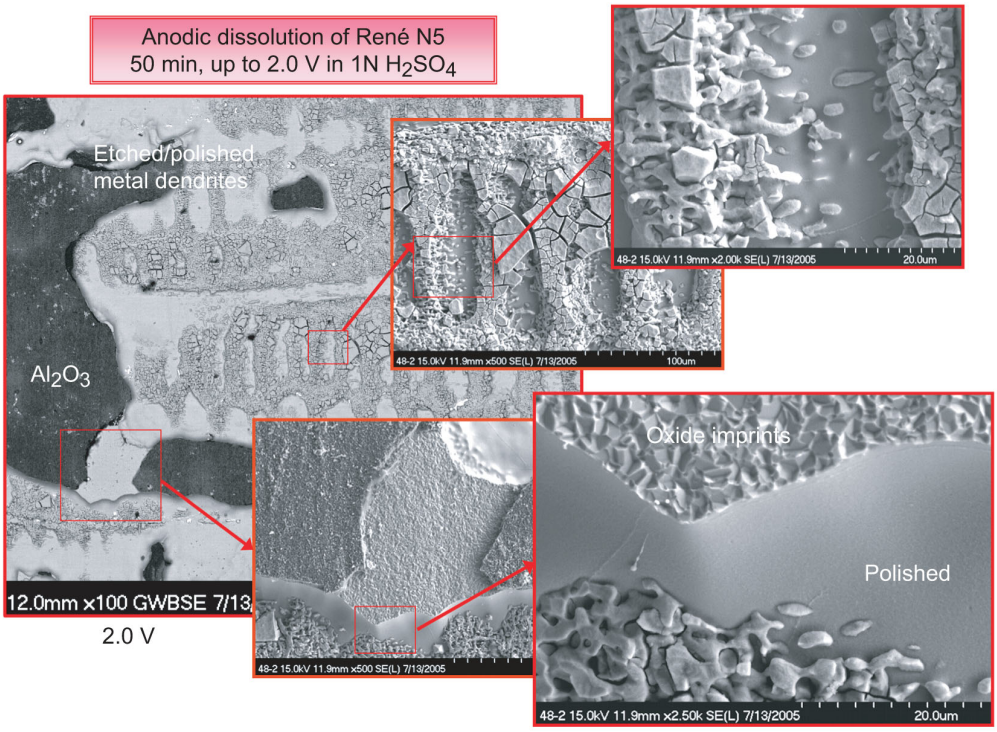

Figure 23.—Montage of SEM/BSE/SEI microstructures after anodic dissolution in 1N H_2SO_4 at 2.0 V for 50 min showing: retained Al_2O_3 scale, electropolished, etched, and craze-cracked alloy structure. (René N5+Y oxidized at 1150 °C, 1000 1-hr cycles).

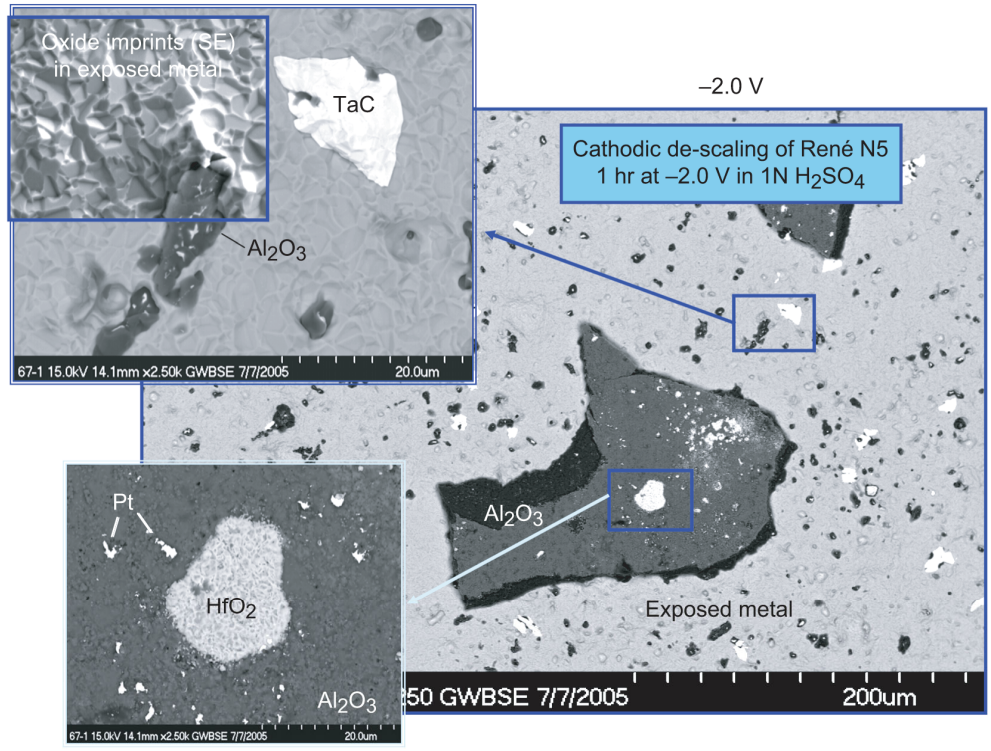

Figure 24.—Montage of SEM/BSE/SEI microstructures after cathodic de-scaling in 1N H_2SO_4 at –2.0 V for 1 hr showing: a limited amount of (dark) retained Al_2O_3 scale (mostly as dispersed particles with (light) HfO_2 overgrowths and Pt particles) and major areas of spalling to (bright) bare metal, revealing oxide imprints and (white) TaC particles. (René N5+Y oxidized at 1150 °C, 1000 1-hr cycles).

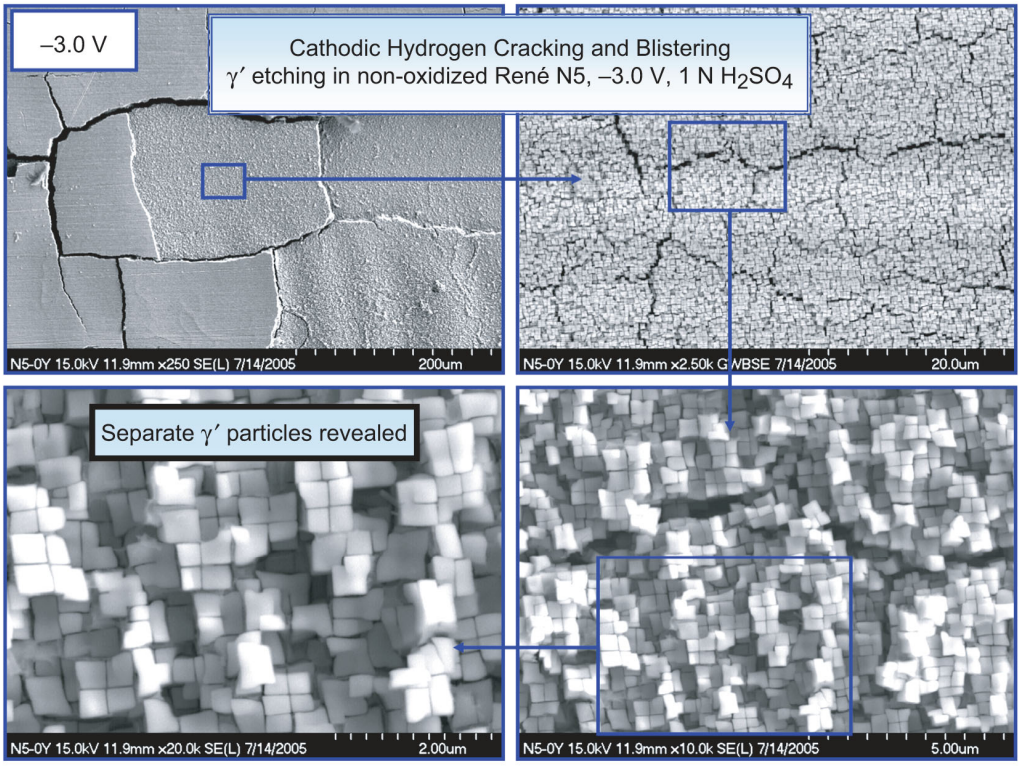

Figure 25.—Structures at increasing magnifications resulting from –3.0 V cathodic charging in 1N H_2SO_4 of unoxidized René N5, showing macrocracks, blisters,γ/γ′ interfacial disruption.

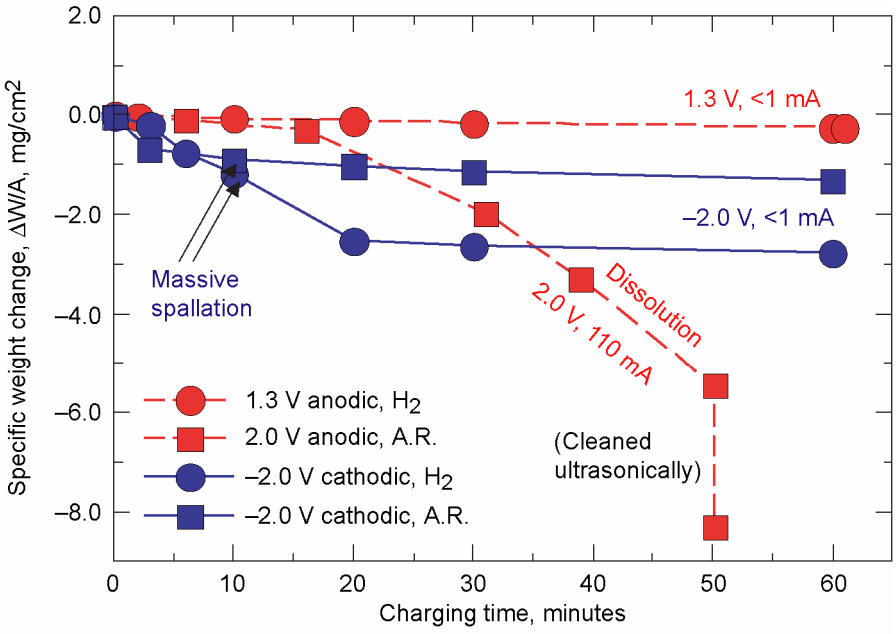

Figure 26.—Weight loss kinetics from anodic dissolution and cathodic de-scaling treatments in 1N H_2SO_4. Note small anodic effects below 2 V and large cathodic effects in the first 20 min.

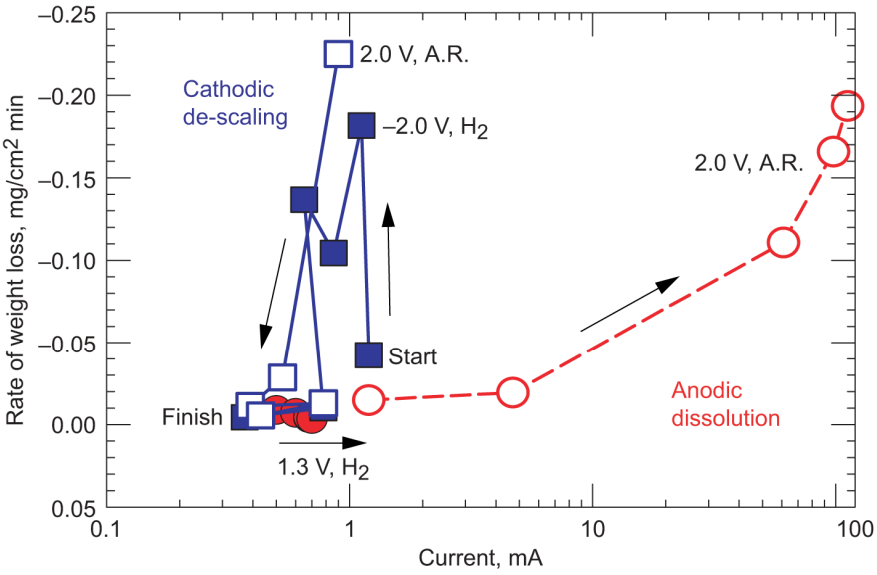

Figure 27.—Approximate rate of weight loss as a function of imposed current for polarization exposures in 1N H_2SO_4: increasing with increasingly higher anodic current; contrasted with discontinuous, initial spikes at comparatively low cathodic currents. (René N5+Y oxidized at 1150 °C, 1000 1-hr cycles).

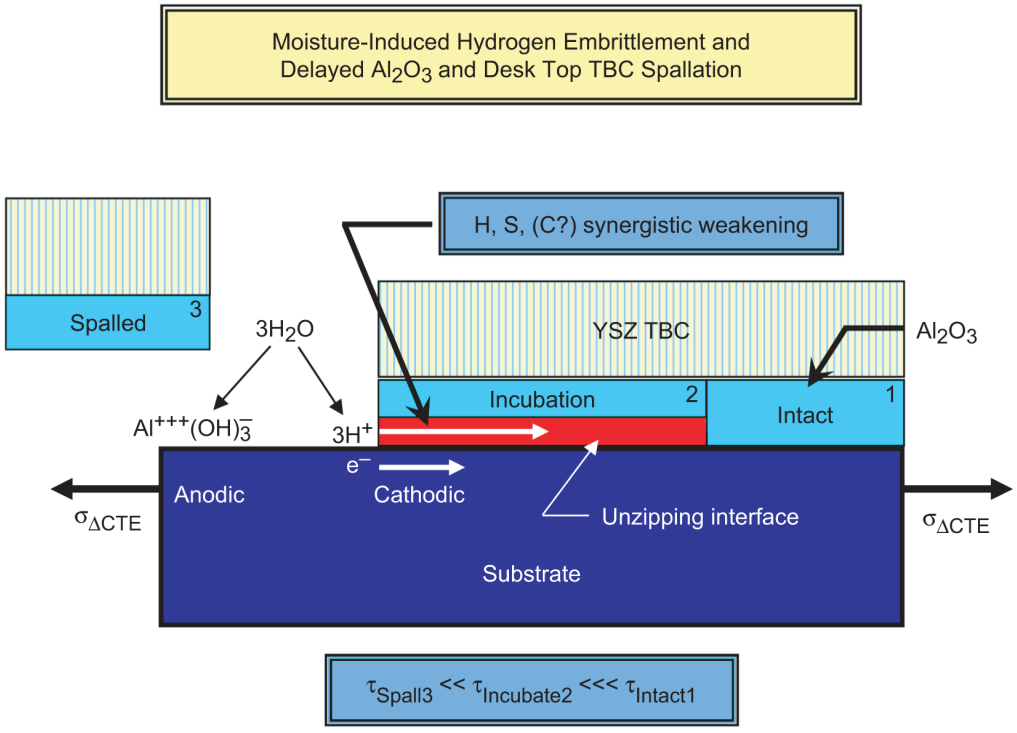

Figure 28.—Schematic of moisture-induced hydrogen embrittlement mechanism used to explain delayed failure of Al_2O_3 scales and desktop TBC spallation: A marginal Al_2O_3-metal interface, under high stress, is exposed to a moist environment; local electrochemical cells produce $(OH)^-$ to react with Al, leaving $(H)^+$ to diffuse into the interface. With time the interface is further weakened and spallation is allowed to occur.

REPORT DOCUMENTATION PAGE

Form Approved
OMB No. 0704-0188

1. AGENCY USE ONLY (*Leave blank*)	2. REPORT DATE	3. REPORT TYPE AND DATES COVERED
	December 2005	Technical Memorandum

4. TITLE AND SUBTITLE

Moisture-Induced Spallation and Interfacial Hydrogen Embrittlement of Alumina Scales

5. FUNDING NUMBERS

WBS–22–714–30–09

6. AUTHOR(S)

James L. Smialek

7. PERFORMING ORGANIZATION NAME(S) AND ADDRESS(ES)

National Aeronautics and Space Administration
John H. Glenn Research Center at Lewis Field
Cleveland, Ohio 44135–3191

8. PERFORMING ORGANIZATION REPORT NUMBER

E–15385

9. SPONSORING/MONITORING AGENCY NAME(S) AND ADDRESS(ES)

National Aeronautics and Space Administration
Washington, DC 20546–0001

10. SPONSORING/MONITORING AGENCY REPORT NUMBER

NASA TM—2005-214030

11. SUPPLEMENTARY NOTES

Prepared for High Temperature Corrosion sponsored by Gordon Research Conferences, New London, New Hampshire, July 24–29, 2005. Responsible person, James L. Smialek, organization code RX, 216–433–5500.

12a. DISTRIBUTION/AVAILABILITY STATEMENT

Unclassified - Unlimited
Subject Categories: 25, 26, and 27

Available electronically at http://gltrs.grc.nasa.gov

This publication is available from the NASA Center for AeroSpace Information, 301–621–0390.

12b. DISTRIBUTION CODE

13. ABSTRACT ***(Maximum 200 words)***

Thermal expansion mismatch stresses and interfacial sulfur activity are the major factors producing primary Al_2O_3 scale spallation on high temperature alloys. However, moisture-induced delayed spallation appears as a secondary, but often dramatic, illustration of an additional mechanistic detail. A historical review of delayed failure of alumina scales and TBC's on superalloys is presented herein. Similarities with metallic phenomena suggest that hydrogen embrittlement from ambient humidity, resulting from the reaction $Al+3H_2O=Al(OH)_3+3H^++3e^-$, is the operative mechanism. This proposal was tested by standard cathodic hydrogen charging in 1N H_2SO_4, applied to Rene'N5 pre-oxidized at 1150 °C for 1000 1-hr cycles, and monitored by weight change, induced current, and microstructure. Here cathodic polarization at –2.0 V abruptly stripped mature Al_2O_3 scales at the oxide-metal interface. Anodic polarization at +2.0 V, however, produced alloy dissolution. Finally, with no applied voltage, the electrolyte alone produced neither scale spallation nor alloy dissolution. These experiments thus highlight the detrimental effects of hydrogen charging on alumina scale adhesion. It is proposed that interfacial hydrogen embrittlement is produced by moist air and is the root cause of both moisture-induced, delayed scale spallation and desktop TBC failures.

14. SUBJECT TERMS

Electrochemistry; Metallic and ceramic materials; Coatings

15. NUMBER OF PAGES

35

16. PRICE CODE

17. SECURITY CLASSIFICATION OF REPORT	18. SECURITY CLASSIFICATION OF THIS PAGE	19. SECURITY CLASSIFICATION OF ABSTRACT	20. LIMITATION OF ABSTRACT
Unclassified	Unclassified	Unclassified	